JGR Atmospheres

RESEARCH ARTICLE
10.1029/2024JD043134

Long-Term Variability and Tendencies of the Semidiurnal Tide in Mesosphere and Lower Thermosphere From Meteor Radar Observations Over Esrange (67.9°N, 21.1°E)

K. Ramesh[1], Nicholas J. Mitchell[1,2], Neil P. Hindley[3], and Tracy Moffat-Griffin[1]

[1]British Antarctic Survey (BAS), Cambridge, UK, [2]Centre for Atmospheric and Environment Research, University of Bath, Bath, UK, [3]Centre for Climate, Adaptation and Environment Research, University of Bath, Bath, UK

Key Points:

- The long-term variabilities in U_{12} and V_{12} are investigated in response to potential drivers in Arctic mesosphere and lower thermosphere for 1999–2022 over Esrange
- The monthly tidal (U_{12} and V_{12}) variabilities are significantly correlated with O_3 in mid-late winter and early spring (January–March)
- The interannual variability and trends of U_{12} and V_{12} are found to vary with altitude and month or season

Correspondence to:
K. Ramesh,
karanamram@gmail.com;
ramara@bas.ac.uk

Citation:
Ramesh, K., Mitchell, N. J., Hindley, N. P., & Moffat-Griffin, T. (2025). Long-term variability and tendencies of the semidiurnal tide in mesosphere and lower thermosphere from meteor radar observations over Esrange (67.9°N, 21.1°E). *Journal of Geophysical Research: Atmospheres*, *130*, e2024JD043134. https://doi.org/10.1029/2024JD043134

Received 9 DEC 2024
Accepted 8 MAR 2025

Abstract Long-term variability and tendencies in monthly mean semidiurnal tide (12-hr) in zonal (U_{12}) and meridional (V_{12}) winds are investigated in northern polar mesosphere and lower thermosphere (MLT; ~80–100 km) using meteor radar observations during 1999–2022 over Esrange (67.9°N, 21.1°E). The climatological mean of U_{12} and V_{12} amplitudes peak (up to ~35 m/s) in winter (December–February) above ~90–95 km with secondary maxima in late summer/early autumn (August–September), however the amplitude of V_{12} is larger than U_{12}. The U_{12} and V_{12} exhibit strong interannual variability that varies with altitude and month/season. The responses of U_{12} and V_{12} anomalies (from 1999–2003) to solar cycle (SC), Quasi Biennial Oscillation (QBO) at 10 hPa and 30 hPa, El Niño-Southern Oscillation (ENSO), North Atlantic Oscillation (NAO), ozone (O_3) and carbon dioxide (CO_2) are analyzed using multiple linear regression. From the analysis, significant correlations are found between monthly tidal amplitudes and the above potential drivers, and the correlations vary with altitude and month. The U_{12} and V_{12} responses to O_3 are positive and significantly large (~60–80 m/s/ppmv) below ~85–90 km in February–March and above ~95 km in January-March. The tidal response to ENSO is significantly negative during August-October (above ~90 km) and positive in November-December (above ~85 km) in both components. The cumulative trend in U_{12} is positive below ~93 km and negative above this height peaking at ~97 km. A positive trend in V_{12} increases above ~93 km and maximize at ~98 km. The significant monthly trends vary with altitude in both tidal components.

Plain Language Summary Atmospheric tides are global scale oscillations in wind, temperature, density, and pressure. They grow in amplitude in response to decreasing density with increasing height. The tides play vital role in transferring energy and momentum from their source regions to mesosphere and lower thermosphere (MLT). In the present study, the long-term variability, and tendencies of the monthly mean semidiurnal tide (12-hr) in both zonal (U_{12}) and meridional (V_{12}) wind components are investigated in the northern polar MLT (~80–100 km) from the meteor radar observations during 1999–2022 over Esrange (67.9°N, 21.1°E). The consistent ability of the radar provided unique long-term data set of the polar MLT winds from which the tidal amplitudes are derived for the period of about two solar cycles. The tidal amplitudes show some important characteristic features, interannual variability and trends that vary with month and altitudes. In addition, the influence of potential drivers including solar activity, Quasi Biennial Oscillation (at 10 hPa and 30 hPa), El Niño-Southern Oscillation, North Atlantic Oscillation, ozone, and carbon dioxide on the variability of tidal amplitudes are investigated from the multiple linear regression analysis. The significant variability and tendencies of the tidal amplitudes can be attributed to the above forcings.

1. Introduction

The large-scale dynamics of the mesosphere and lower thermosphere (MLT) are dominated by atmospheric solar tides of large amplitude. They are global-scale oscillations at periods which are subharmonics of a solar day viz., 24-hr (diurnal), 12-hr (semidiurnal) and 8-hr (terdiurnal) etc (Chapman & Lindzen, 1970). They are apparent in basic atmospheric variables including wind, temperature, density, pressure and/or in tidally induced effects such as airglow emissions and trace species (López-González et al., 2017; Smith, 2012). Further the tidal signatures can be determined in noctilucent clouds over middle and high latitudes (Fiedler & Baumgarten, 2018). Tides play crucial role in dynamical coupling of different layers from their source regions to the upper atmosphere including ionosphere and thermosphere. Their amplitude grows with altitude in response to exponentially decreasing density to conserve the energy, and transport momentum and energy into the MLT (e.g., Lieberman et al., 2000;

Pancheva et al., 2009; Smith, 2012) to influence the thermal, dynamical, and chemical processes of this region. Based on migrating (sun-synchronous) and non-migrating (non-sun-synchronous) modes, the tides are predominantly forced by absorption of solar (a) infrared radiation (IR) by tropospheric (~0–15 km) water vapor (H_2O), (b) ultraviolet (UV) radiation by stratospheric and lower mesospheric (~30–60 km) ozone (O_3), (c) extreme ultraviolet (EUV) radiation by molecular oxygen (O_2) and nitrogen (N_2) in the lower thermosphere (~120–170 km) (e.g., Chapman & Lindzen, 1970; Forbes, 1995). The other sources include release of latent heat due to deep tropospheric convection over the tropics, non-linear interaction of tides and planetary waves (Forbes et al., 2007; Hagan & Forbes, 2002, 2003; Oberheide et al., 2002; Vadas et al., 2014) and land-sea contrast of solar heating (Kato et al., 1982). In the MLT, the tidal amplitudes exhibit significant variability that depends on latitude, altitude, and season. For example, the diurnal tides are more prominent over tropical-low latitudes with maximum amplitudes at around 95 km (e.g., Ramesh & Smith, 2021; Ramesh et al., 2020; Smith, 2012), while the semidiurnal tides are dominant over middle and high latitudes (Manson et al., 2002; Pancheva et al., 2009; Wu et al., 2011) with their largest amplitudes above mesopause (Smith, 2012). The terdiurnal tides are smaller than the diurnal and semidiurnal tides and show peak amplitudes over middle latitudes above ~95 km (e.g., Pancheva et al., 2013; Smith, 2000; Yue et al., 2013). Tides can control the vertical propagation of the gravity waves (GWs) through filtering effect of the tidal winds (Fritts & Vincent, 1987) and influence the wave induced momentum flux and thereby the atmospheric circulation (Fritts & Alexander, 2003; Yiğit et al., 2021). However, the interaction of the GWs can amplify or damp the tidal amplitudes when they break at various tidal phases (Smith, 2012). Further tides play a significant role in the diurnal cycle and vertical transport of the chemically active species (e.g., Marsh & Russell, 2000; Ward, 1999; Zhang et al., 2001) which in turn influence the chemical heating in the MLT (Smith et al., 2003).

Among the broad spectrum of vertically propagating atmospheric waves, tides continue to be a major focus of MLT research over the past three decades emphasizing their important role in dynamical coupling of the lower and upper atmosphere. Various ground based (meteor radar, medium frequency radar and lidar) and spaceborne observations are helpful to reveal the important characteristics including the structure and variabilities (including seasonal and interannual) of the tides (24-hr, 12-hr, 8-hr) over low-, mid- and high-latitudes. The ground-based observations provide the vertical wavelength, direction of propagation (Manson et al., 2004; Mitchell et al., 2002; Pancheva & Mitchell, 2004), seasonal and interannual variabilities of the tides over a specific location while the satellite observations provide the global structure of the tides and distinguish the migrating and nonmigrating components (e.g., Pancheva et al., 2009; Pancheva & Mukhtarov, 2011). However, the numerical models are capable of reproducing the seasonal and global tidal fields (Achatz et al., 2008; Akmaev et al., 2008; Chang et al., 2008; Covey et al., 2014; Gan et al., 2014; Grieger et al., 2002; Hagan et al., 1995, 1999, 2001; Hagan & Forbes, 2002, 2003; Lu et al., 2012; McLandress, 2002; Miyahara et al., 1999; Oberheide et al., 2011; Pedatella et al., 2021; Ramesh & Smith, 2021; Ramesh et al., 2020; Smith, 2012; Ward et al., 2005) to study the long-term and interannual variabilities.

Although the diurnal tide is dominant in the tropical-low latitude MLT, it weakens over mid-latitudes and trapped in the high-latitude stratosphere. The semidiurnal tide, maximizing in the mid-high latitude MLT winds, is a main driver of diurnal, inter-seasonal and interannual variabilities of this region (e.g., Arras et al., 2009; Pancheva et al., 2009; Shepherd et al., 1998; Van Caspel et al., 2022). Recently Goncharenko et al. (2023) emphasized the importance of the semidiurnal tide to influence the ionosphere-thermosphere-mesosphere (ITM) system and for the lower-upper atmosphere coupling. They further stressed the potential need of understanding of the semidiurnal tidal variability which is lacking mainly due to the observational limitations. Pancheva et al. (2009) have briefed several previous studies that revealed the important features and variabilities (short-term, seasonal, and long-term) of the semidiurnal tide from ground based and spaceborne observations, and model simulations. The long-term variabilities of the semidiurnal tide in MLT are believed to occur due to several important mechanisms including (a) variations in the tidal forcing in the troposphere and stratosphere, (b) vertical propagation characteristics modulated by the background wind and temperature in the middle atmosphere (stratosphere and mesosphere), (c) non-linear interaction with gravity waves and planetary waves, and (d) variations in the solar flux and geomagnetic activities. The understanding of the semidiurnal tidal characteristics and variabilities in the MLT region is significantly improved due to several space-borne (e.g., TIMED-SABER: Thermosphere Ionosphere Mesosphere Energetics Dynamics—Sounding of the Atmosphere using Broadband Emission Radiometry and TIDI: TIMED Doppler Interferometer) and ground-based (e.g., VHF radars) observations, and model simulations. However, the knowledge of the potential sources for the significant variabilities (long-term and

interannual) of the semidiurnal tide is inadequate especially over high latitudes. Very few studies have focussed on these aspects (e.g., Dempsey et al., 2022; Pancheva et al., 2002), but none of them include all possible drivers that are responsible for the semidiurnal tidal variability especially in the polar MLT.

The significant interannual, seasonal and long-term variabilities of the semidiurnal tides in the polar MLT are believed to be mainly driven by the solar cycle, Quasi-Biennial Oscillation (QBO), El Niño Southern oscillation (ENSO), North Atlantic Oscillation (NAO in the northern hemisphere), O_3 and CO_2. The incoming solar flux variations strongly influence the tidal variability in the middle atmosphere and lower thermosphere because the major migrating tidal components are forced mainly through the solar heating due to water vapor and ozone in the troposphere and stratosphere. Moreover, the solar flux variability significantly modulates the background temperature and thereby the winds that influence the tidal vertical propagation conditions. Pancheva et al. (2009) indicated that the variability in semidiurnal tidal amplitudes could be due to the variations in the solar activity and the total ozone. The QBO in the equatorial/tropical lower stratospheric zonal wind can significantly influence the MLT neutral winds and tides through dynamical coupling globally (e.g., Gurubaran & Rajaram, 1999, Forbes et al., 2008; Laskar et al., 2016; Wu et al., 2008). Hibbins et al. (2007) illustrated the enhancement of the southern high-latitude semidiurnal tidal amplitudes during eastward phase of the QBO. Pancheva et al. (2009) noted the interannual variability of the semidiurnal tide in the mid-latitude lower thermosphere can be driven by the QBO. Laskar et al. (2016), from the meteor radar observations over two northern mid-, and high-latitude stations, reported the enhancement of the mesospheric semidiurnal tidal amplitudes below and above mean level for the QBO westward and eastward phases. One of the potential sources for the long-term and interannual variability in the MLT tides is the ESNO (e.g., Gurubaran et al., 2005; Lieberman et al., 2007; Liu et al., 2017; Oberheide et al., 2011; Ramesh & Smith, 2021; Ramesh et al., 2020; Sundararajan, 2020). Pedatella and Liu (2012) simulated the diurnal and semidiurnal tidal variability in MLT driven by the ENSO. They found the enhancement of the semidiurnal tidal (SW4) amplitude during the El Niño phase of the ENSO.

The NAO, a regional scale tropospheric circulation over Atlantic and Europe, is another potential driver of the atmospheric variability (e.g., Kolstad et al., 2020) connecting the polar stratosphere and mesosphere via dynamical coupling (e.g., Jacobi & Beckmann, 1999). The link between NAO and stratospheric polar vortex could be useful for the detection of long-term variability in the MLT winds and tides over this region. There have been very few reports that link the variability in polar MLT winds and tides with the NAO. As the NAO signal correlates with the mesopause/MLT winds over northern polar latitudes (e.g., Jacobi & Beckmann, 1999; Ramesh et al., 2024), it is strongly believed that the NAO profoundly impacts the tidal oscillations of this region. The ozone is an important driver of the polar semidiurnal tidal variability because its absorption of solar ultraviolet radiation mainly generates the migrating semidiurnal tide (westward zonal wavenumber 2, SW2) (e.g., Forbes & Garrett, 1978; Lindzen & Chapman, 1969). Hence any changes in the stratospheric ozone can significantly influence the variations in the tidal amplitudes in the MLT. For example, Siddiqui et al. (2019) simulated the increase in stratospheric ozone during 2009 sudden stratospheric warming event could potentially enhance the amplitude of the semidiurnal tide in the MLT region. The CO_2 is an important driver of the radiative cooling in the middle atmosphere and lower thermosphere. The changes in temperature and composition due to increasing CO_2 have direct impact on the MLT winds and tides (e.g., Laštovička et al., 2008; Ramesh & Smith, 2021; Ramesh et al., 2020). Although the increasing trend in MLT diurnal tide is predominantly due to increasing CO_2 (Ramesh et al., 2020), however, the effect of long-term increase of CO_2 on the semidiurnal tidal variability is least explored especially over the polar latitudes where their amplitudes are significantly large.

It is crucial to better understand the dynamical processes and their associated mechanisms in the polar MLT in terms of coupling of the middle and upper boundary of the terrestrial atmosphere. The main scientific goal of this study is to investigate the long-term tendencies and interannual variabilities of the semidiurnal tidal amplitudes in the Arctic MLT zonal (U_{12}) and meridional winds (V_{12}) from the meteor radar observations during 1999–2022 over Esrange (67.9°N, 21.1°E). Further the responses of U_{12} and V_{12} monthly anomalies (from 1999–2003) to the above predominant climate forcings viz., solar cycle (SC), Quasi Biennial Oscillation (QBO) at 10 hPa and 30 hPa, El Niño-Southern Oscillation (ENSO), North Atlantic Oscillation (NAO), ozone (O_3) and carbon dioxide (CO_2) are analyzed using multiple linear regression (MLR). The analysis reveals some important results for better understanding of the variabilities and tendencies in the Arctic MLT semidiurnal tides possibly due to the above most significant drivers during the observational period. This is a companion study of Ramesh et al. (2024) which explores the long-term variabilities and tendencies in the Arctic MLT horizonal winds from the meteor radar observations during 1999–2022 over Esrange in response to the above dominant forcings. Section 2 provides the

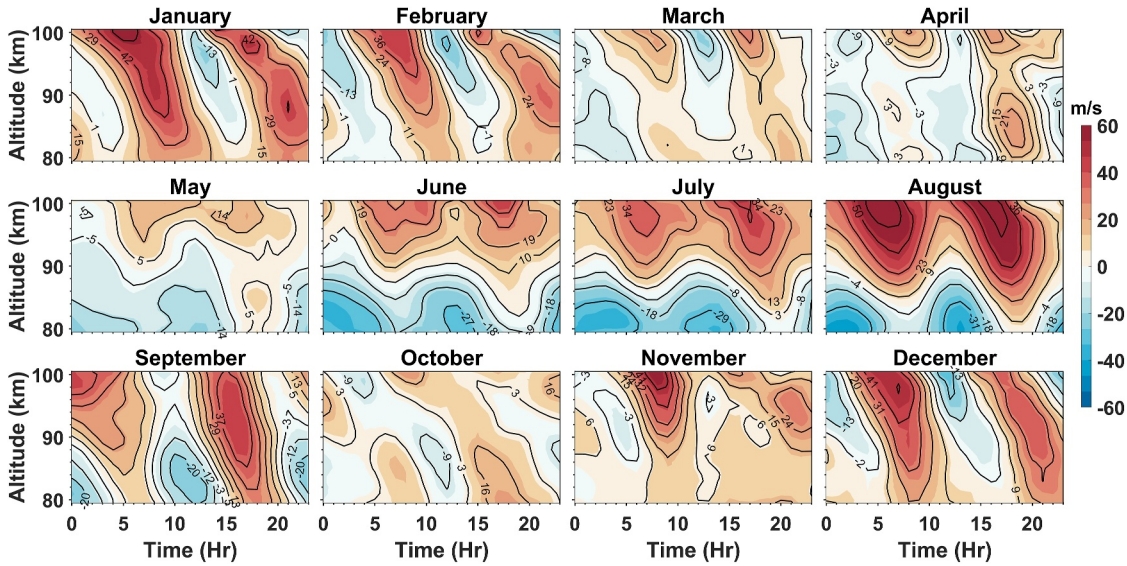

Figure 1. The composite day (in UTC) variations of the MLT zonal winds (U) for each month of the year 2007 at ∼80–100 km over Esrange.

details of data and analysis method, Section 3 presents the results, summary and discussion are detailed in Section 4 and finally the main conclusions of the study are listed in Section 5.

2. Data and Methodology

2.1. Esrange Meteor Radar Data

In this study, the meteor radar observations are used over Esrange (67.9°N, 21.1°E), Sweden for the period of 1999–2022. The radar is a commercially produced all-sky Interferometric SKiYMET VHF system operating continuously from August 1999. It is a pulsed system that uses a transmitter of 6 kW peak power and operates at a frequency of 32.5 MHz with a pulse repletion frequency (PRF) of 2144 Hz and a duty cycle of 15%. Further it uses five receiver aerials which are configured to function as an interferometer to determine the azimuth and elevation angles of meteor echoes required to determine the MLT horizontal winds. The routine measurement of the radar yields the hourly zonal and meridional winds at the typical height resolution of ∼2 km between ∼80 and ∼100 km. Further details about this radar and its observations of mean winds, and tides (diurnal and semidiurnal) can be obtained from Mitchell et al. (2002). The information about meteor detection algorithm can be found in Hocking et al. (2001). Since it is crucial in the studies of long-term variability, the performance of the radar has been carefully examined for any significant changes over the period of the data set. It is found that the basic configuration of the radar persisted with no significant changes since the installation of the system (Ramesh et al., 2024). Thus, it is well suited for investigating the long-term variability in the MLT tidal winds as no major biases arose in the radar observations. Since the commencement of its observations, the radar has been operational till date (in 2024), however there exist a few data gaps as shown in Figure 1f and Figure S2 of Ramesh et al. (2024) primarily due to technical problems and when the radar was unable to operate. More information about the distribution and detection of the meteors using this radar for the observational period can be found in Ramesh et al. (2024).

2.2. Analysis Method

2.2.1. Tidal Amplitude and Phase

For investigating the long-term variabilities of the semidiurnal tides, their amplitudes are retrieved from the hourly zonal and meridional winds of the meteor radar observations over Esrange for 1999–2022. The improved time-height localisation of the meteor radar winds has been acquired from the Gaussian-weighting approach. This method uses Guassian-weighted least squares fit to improve the accuracy in deriving the hourly horizontal winds in the MLT. A complete description of this new improved method (when compared to a traditional height gates approach) is given by Hindley et al. (2022). The seasonal, interannual and long-term variabilities in the monthly

zonal and meridional winds derived from this method for the same observational period over Esrange can be seen in Ramesh et al. (2024). In this study, the sliding composite day method (also known as superposed epoch analysis) is used to determine the tidal characteristics. The radar detected meteors within a specified range of days before and after a particular day are anticipated to have been measured on that same day. The Gaussian-weighted wind fitting method is adopted to generate a composite day of hourly winds at each height for all the observations. To derive the amplitude and phase of the semidiurnal tide, a least-squares fit of a specific sinusoidal oscillation of period 12-hr is made to the composite day (sliding 30-day composite window) wind time series at each height between ∼80 and ∼100 km. The sinusoidal fitting is made as per the Equation 4 of Hindley et al. (2022). For hourly zonal (U) and meridional (V) winds at one height, this can be given as follows.

$$U(t), V(t) = A_{12}\ \cos\left(\frac{2\pi t}{T}\right) + B_{12}\ \sin\left(\frac{2\pi t}{T}\right) + C \tag{1}$$

Here t contains the weighted average times of the hourly wind measurements in hours and T is the tidal period (here $T = 12$ hr). The amplitude and phase of the semidiurnal tide are given by $\sqrt{A_{12}^2 + B_{12}^2}$ and $\tan^{-1}\left(\frac{B_{12}}{A_{12}}\right)$ with A_{12} and B_{12} representing the tidal amplitude coefficients for the cosine and sine terms respectively. The C is the mean background wind for the composite day. This process is repeated to fit at all the heights between ∼80 and ∼100 km.

2.2.2. Multiple Linear Regression

The long-term variability and tendencies in the monthly mean semidiurnal tidal amplitudes in response to the natural and anthropogenic forcing are retrieved from multiple liner regression (MLR) analysis. The monthly tidal and predictor anomalies are calculated with respect to the first five years of the observations, 1999–2003 that is, the difference between the value in a specific month and the average of all values over this 5 years period for that month. The MLR analysis determines the responses of the changes in tidal amplitudes to the potential drivers of SC, QBO, ENSO, NAO, O_3, and CO_2. The general expression for the regression model is given below.

$$\varphi(t) = \alpha + \sum_{i=1}^{n} \beta_i K_i(t) + \varepsilon(t) \tag{2}$$

where φ is the predictand, that is, ΔU_{12} or ΔV_{12}, t is the time in months, α is a constant, β_i are regression coefficients corresponding to n predictors (here $n = 7$), K is a matrix containing n predictors, and ε is the residual. The matrix K includes the following seven predictors.

$$K = \begin{pmatrix} F_{10.7} \\ \text{QBO10} \\ \text{QBO30} \\ \text{NINO 3.4} \\ \text{NAO} \\ O_3 \\ CO_2 \end{pmatrix} \tag{3}$$

where $F_{10.7}$ is the 10.7 cm solar radio flux which is the proxy for solar activity in solar flux units (sfu), 1 sfu $= 10^{-22}$ $Wm^{-2}Hz^{-1}$; QBO10 and QBO30 are the zonal mean zonal winds (m/s) averaged over 5°N–5°S at 10 and 30 hPa respectively; NINO 3.4 index, the proxy for ENSO, is equatorial Pacific Sea surface temperature (K) averaged over 5°N–5°S and 170°W–120°W; The NAO index is the difference in normalized sea level pressures between Ponta Delgadas (Azores) and Akureyri (Iceland); O_3 is the global mean of ozone volume mixing ratio (VMR) in ppmv at 1 hPa (∼48 km); and CO_2 is the global average of surface carbon dioxide volume mixing ratio in ppmv. More details about these regressors can be found in Ramesh et al. (2024). The regressors of monthly

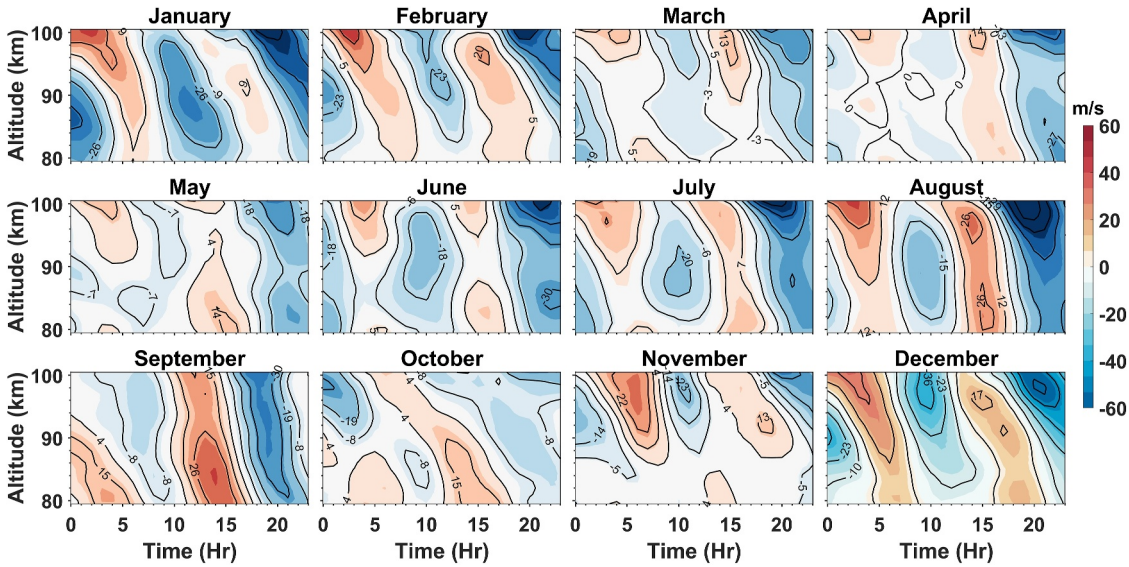

Figure 2. Same as Figure 1, but for meridional winds (V).

mean changes (with respect to 1999–2003) are used in the MLR analysis to obtain the regression coefficient/response of each predictor. It should be noted that the data gaps are included in the regressors for the months/years corresponding to that in the radar wind/tidal observations to avoid any misleading results from the regression analysis.

3. Results

3.1. Tidal Signatures in MLT Winds

The basic tidal signatures in the MLT winds can be detected through the diurnal variability of the winds in the height domain. For example, Figures 1 and 2 represent the composite day (in UTC) variations of the MLT zonal (U) and meridional (V) winds respectively for each month of the year 2007 at ~80–100 km over Esrange. Here the composite days are created for each month to generate a representative day for that month. By visual inspection, the winds exhibit a clear semidiurnal (12-hr) oscillation in both the components with strong tidal winds (up to ~60 m/s including background winds underlying tides) found in August-September and December-January. Further to detect and characterize the tidal periodicities, the MLT winds are diagnosed with Lomb-Scargle (L-S) periodogram. Figure 3 illustrates the normalized L-S periodogram of hourly zonal and meridional winds at 90 km for the period of August 1999–December 2022. The power spectra indicate the large semidiurnal (12 hr) tide

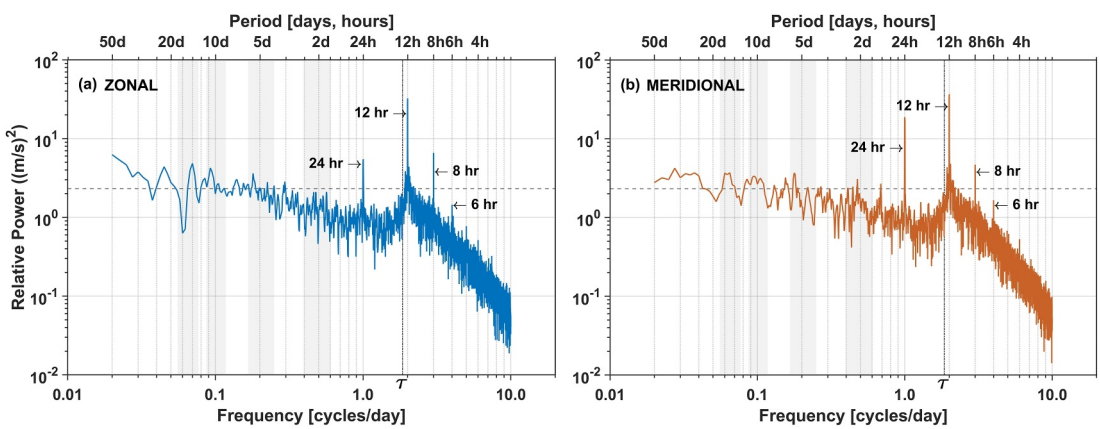

Figure 3. Normalized power spectra of hourly (a) zonal and (b) meridional winds at 90 km for 1999–2022 over Esrange. The dashed horizontal line represents the 90% confidence level and τ denotes the inertial period (~12.9 hr). The tidal periods (24, 12, 8, and 6 hr) are marked in both panels of the figure.

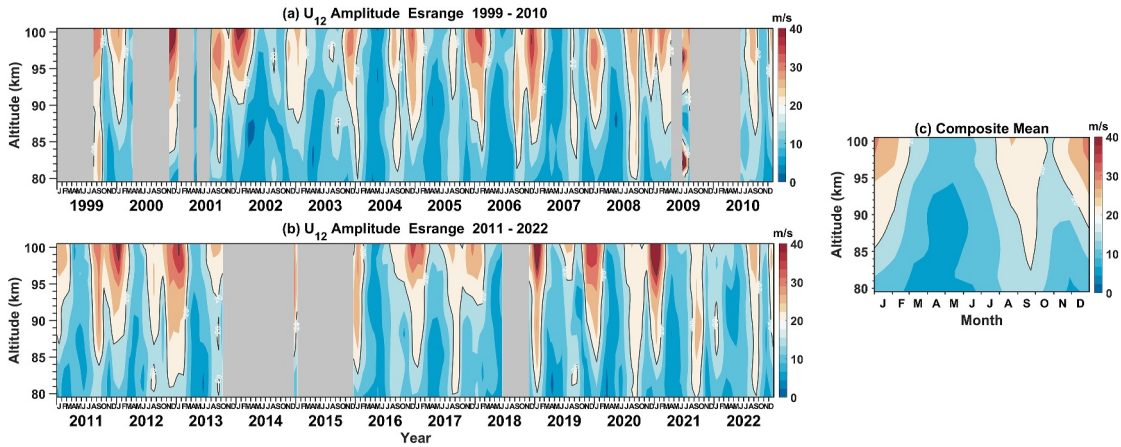

Figure 4. Monthly amplitudes of the semidiurnal tide in zonal wind (U_{12}) for (a) 1999–2010, (b) 2011–2022, and (c) their composite means in the MLT region (~80–100 km) from the meteor radar observations over Esrange. The vertical gray patches in (a, b) indicate the data gaps.

dominates in both wind components with the diurnal (24 hr) tide being the secondary in the meridional winds over Esrange. The amplitude of the semidiurnal tide is nearly consistent in U and V whereas the diurnal tidal amplitude is much larger in V than in U. The amplitude of the terdiurnal (8 hr) tide is almost equal to that of the diurnal tide in zonal winds, but it is much smaller in the meridional winds. The power spectra also show the quarterdiurnal tide (6 hr), however its amplitude is below the 90% significant level (horizontal dashed line). Apart from the tidal periods, the gravity waves with periods shorter than the inertial period ($\tau \sim 12.9$ hr at this location) can be seen in the power spectra of both wind components. The present study focuses on the largest tide, that is, 12-hr tide only.

3.2. Climatology of the Semidiurnal Tide

3.2.1. Tidal Amplitude

The variations of the monthly mean semidiurnal tidal amplitude in zonal winds (U_{12}) for the height region of ~80–100 km during 1999–2022 over Esrange are depicted in Figures 4a and 4b. The vertical gray patches in both the panels indicate the data gaps that arose due to non-availability of the meteor radar observations. It can be observed from the figure that the tidal amplitude increases with altitude and exhibits strong interannual variability. For example, it ranges from ~20 m/s in 2002, and ~30 m/s in 2005 and 2006 to the maximum of ~40 m/s in 2018, 2020 above ~95 km in the winter months (December–January). The interannual variability in the tidal amplitude also exists during August-October varying from ~20 m/s in 2005, 2007, 2020 to a maximum of ~30 m/s in 1999, 2001, 2011. Figure 4c illustrates the composite mean (averaged for all the years) of monthly tidal amplitudes at ~80–100 km. From the figure, it can be observed that the tidal amplitudes are least in spring (March–May) below ~95 km and in late autumn/early winter (November-December) at lowermost altitudes. However, the tidal amplitudes are large (~30–35 m/s) in winter months (December–February) above ~95 km with secondary maximum (~20–25 m/s) during late summer and early autumn (August-October) above ~82 km.

The monthly variations of the semidiurnal tidal amplitude in the meridional wind (V_{12}) at ~80–100 km over Esrange are shown in Figures 5a and 5b for the observational period. The vertical gray patches represent the data gaps in both panels. It can be observed that the V_{12} also exhibit significant interannual variability; for example, the winter amplitudes range from ~30 m/s in 1999, 2007, 2015 to the maximum of ~40 m/s in 2001, 2006, 2016, 2018, 2020 above ~95 km. In addition, the V_{12} exhibits significant interannual variability during August-September with the amplitudes range from ~25 m/s in 2002 to ~35 m/s in 2004, 2016, 2017 with a maximum of ~40 m/s in 2008 above ~95 km. Figure 5c depicts the composite mean monthly amplitudes of V_{12} at ~80–100 km. It can be observed that the tidal amplitudes are minimum in spring below ~95 km, however they are significantly large (~30–35 m/s) above this height in winter and late summer and early autumn (August–September).

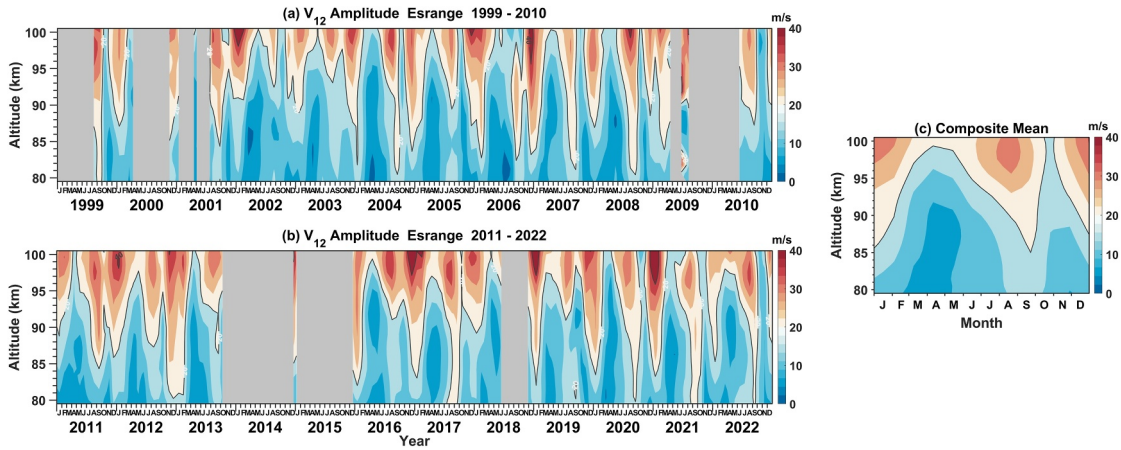

Figure 5. Same as Figure 4 but for semidiurnal tide in meridional wind (V_{12}).

3.2.2. Tidal Phase

The monthly mean variabilities of the semidiurnal tidal phases in the zonal and meridional components are presented in Figures 6 and 7 respectively. The zonal and meridional tidal phases are defined as the time (in hours) of first maximum of the eastward wind and the northward wind respectively, measured in local time. It is likely that the tidal phase values are larger (i.e., later hours)/smaller (i.e., early hours) when the amplitudes of the tide are relatively small/large (Figures 4 and 5) in both the components. Further it is obvious that a negative change in tidal phase with increasing height when the tidal amplitudes are relatively large, signifying the upward propagating tide. These features are more pronounced in the late winter (January–February) and autumnal equinox (September–November). In addition, when the tidal amplitudes are larger, the meridional phase lags the zonal by a quarter cycle. Like the tidal amplitudes, phases in both the components exhibit interannual and seasonal variability. The tidal phase in both the components is nearly constant (i.e., the variability is considerably small) during April-August at all heights, then decreases to early hours in the autumnal equinox and proceeds to later hours in the early winter (December), finally attaining the latest hours in the late winter (January–February). These seasonal variations in the tidal phases are consistent with that reported by Mitchell et al. (2002) using 1 year of meteor radar observations during August, 1999–July, 2000 over Esrange. They found the phase difference between the two tidal components was around ∼3 hr at all observational heights in all the months representing the phase quadrature.

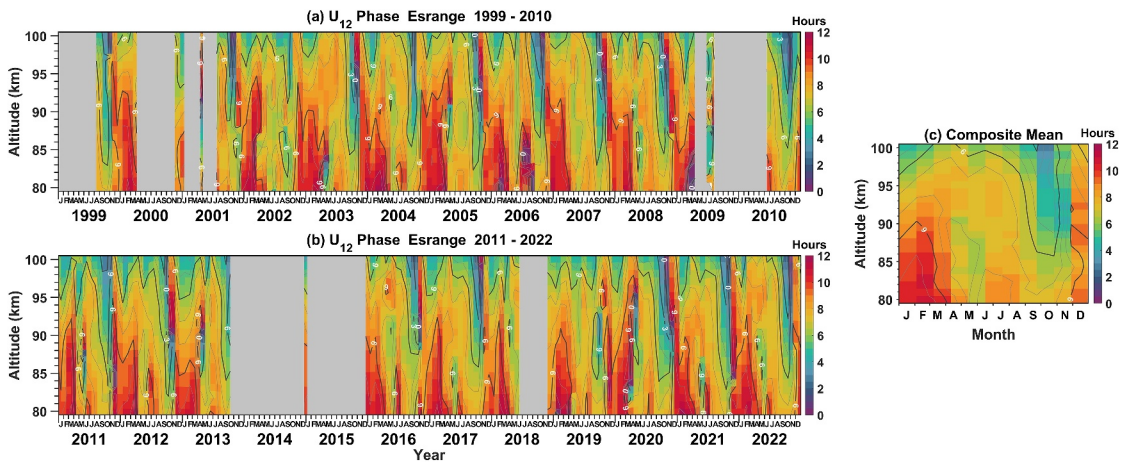

Figure 6. Monthly phases of the semidiurnal tide in zonal wind (U_{12}) for (a) 1999–2010, (b) 2011–2022, and (c) their composite means in the MLT region (∼80–100 km) from the meteor radar observations over Esrange. Here the phases are given in hours since midnight local time. The vertical gray patches in (a, b) indicate the data gaps.

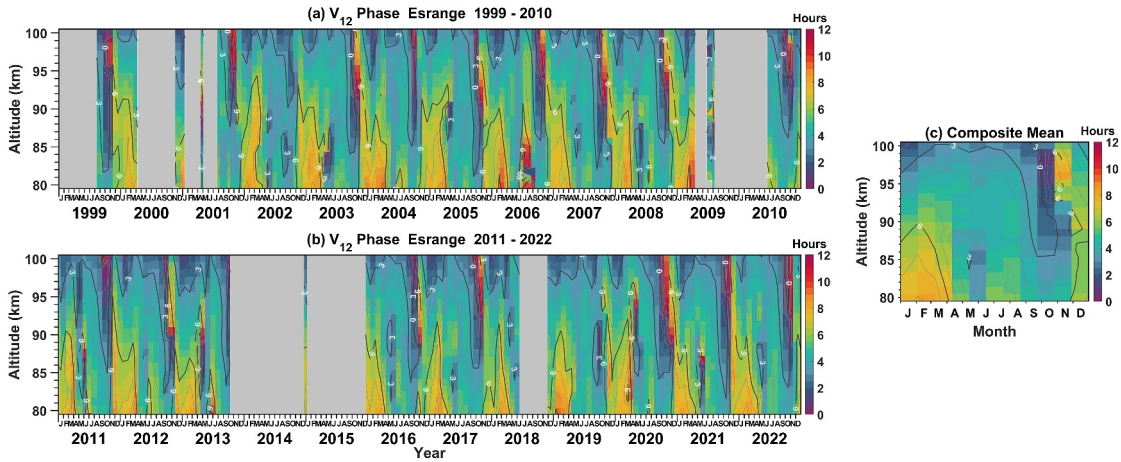

Figure 7. Same as Figure 6 but for semidiurnal tide in meridional wind (V_{12}).

3.3. Interannual Variability of the Semidiurnal Tide

The interannual variabilities of the semidiurnal tidal amplitudes in both zonal (U_{12}) and meridional (V_{12}) components for each month at two different heights, 89.9 km, and 98.5 km for 1999–2022 are shown in Figure 8.

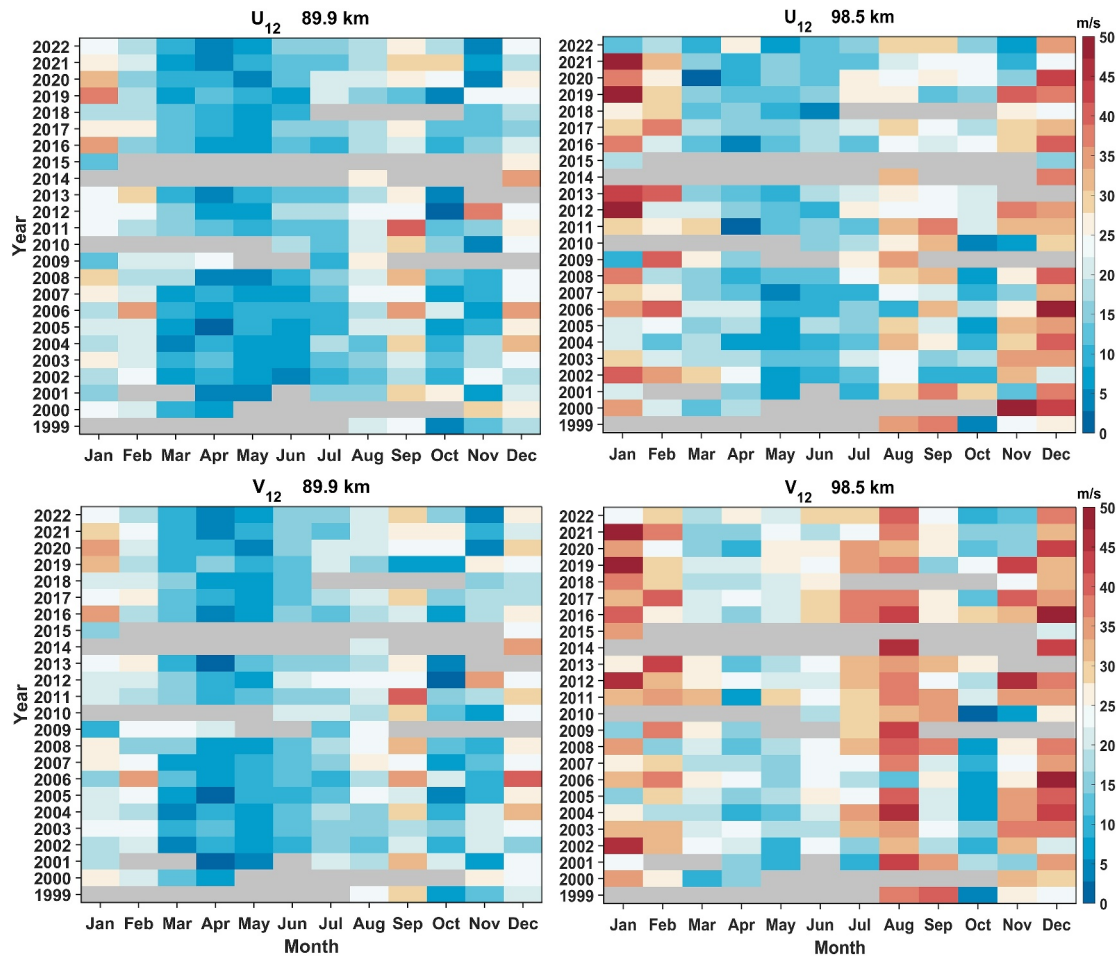

Figure 8. Year-to-year variability of the amplitudes of (top) zonal semidiurnal tide (U_{12}) and (bottom) meridional semidiurnal tide (V_{12}) for each month at two different heights of (left) 89.9 km and (right) 98.5 km during 1999–2022 over Esrange. The gray pixels in the figure panels denote the observational data gaps.

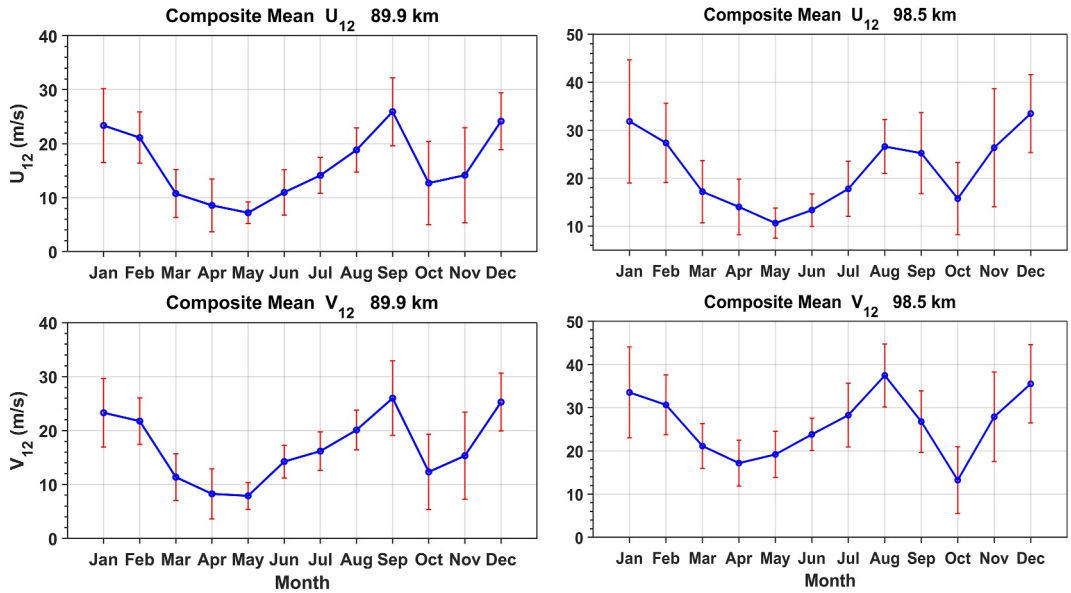

Figure 9. Monthly variation of composite mean amplitudes of (top) zonal semidiurnal tide (U_{12}), and (bottom) meridional semidiurnal tide (V_{12}) (in blue) at two different heights, (left) 89.9 km and (right) 98.5 km. The vertical bars (in red) denote the standard deviations of the tidal amplitudes for each month.

The gray pixels in the figure denote the observational data gaps. It is evident from the figure that there exists substantial interannual variability in both the tidal components in each month at the two height levels. At 89.9 km, the variability in zonal tide is relatively small when the amplitudes are least during spring equinox (March–May). For example, the U_{12} amplitude in April varies from ∼3 m/s in 2005 and ∼10 m/s in 2000, 2012, 2016 to ∼15 m/s in 2003, 2019. The variability is more pronounced when the tidal amplitudes are relatively large during autumnal equinox and in winter. For instance, in September, the tidal amplitude varies by ∼30 m/s between 2011 and 2019; however, it is ∼25 m/s in the month of January between 2009, 2015 and 2019. Similarly at higher altitude of 98.5 km, the variability is small in late spring/early summer (e.g., ∼10 m/s in May between 2007 and 2020, 2021) when the tidal amplitudes are minimum; however, it is more pronounced when the U_{12} amplitudes are relatively strong in the late autumn and winter. In November, the tidal amplitude varies from ∼8 m/s in 2010, 2022 to the maximum of ∼50 m/s in 2000, while it ranges from ∼10 m/s in 2009 to ∼50 m/s in 2012, 2019, 2021 in the month of January. Like U_{12}, the variability in the meridional tide is small when the amplitude is relatively small (March–May) and more pronounced when the tidal amplitude is large (autumn and winter) at both the heights.

Figure 9 illustrates the composite means of all years for the monthly tidal amplitudes in both the components to characterize the interannual variabilities at the same height levels (given in Figure 8) of 89.9 and 98.5 km. The vertical bars (in red) denote the standard deviations for each month to represent the tidal variability in that month. At 89.9 km, the variability (deviation) in the tidal amplitude in both zonal and meridional components is large during March–April (U_{12} ∼ 4.4–4.9 m/s, V_{12} ∼ 4.3–4.6 m/s), October–November (U_{12} ∼ 7.7–8.9 m/s, V_{12} ∼ 7–8 m/s) and in the winter months especially in January (U_{12} ∼ 6.8 m/s, V_{12} ∼ 6.3 m/s). However, it is least in May (U_{12} ∼ 2 m/s, V_{12} ∼ 2.4 m/s) and relatively smaller in summer. At 98.5 km, the tidal variability in both the components is larger during autumn and winter with maximum deviation in November (U_{12} ∼ 12.3 m/s, V_{12} ∼ 10.3 m/s) and January (U_{12} ∼ 12.8 m/s, V_{12} ∼ 10.5 m/s) months. However, it is minimum during May–June (U_{12} ∼ 3.1–3.3 m/s, V_{12} ∼ 3.7–5.3 m/s) in both the components.

3.4. Time Series of Predictors for 1999–2022

The temporal variations of monthly predictors used in the regression model (Equations 2 and 3) for 1999–2022 are depicted in Figure 10. The solar proxy ($F_{10.7}$) includes the 11-year cycles 23, 24 and part of 25 with decreasing solar maxima over this period. The two near orthogonal QBO indices at 10 hPa (QBO10) and 30 hPa (QBO30) vary between 20 m/s and 40 m/s in eastward and westward phases respectively, and no significant long-term trend is apparent in these two indices. The NINO 3.4 index, a proxy for ENSO, shows slight increasing trend during

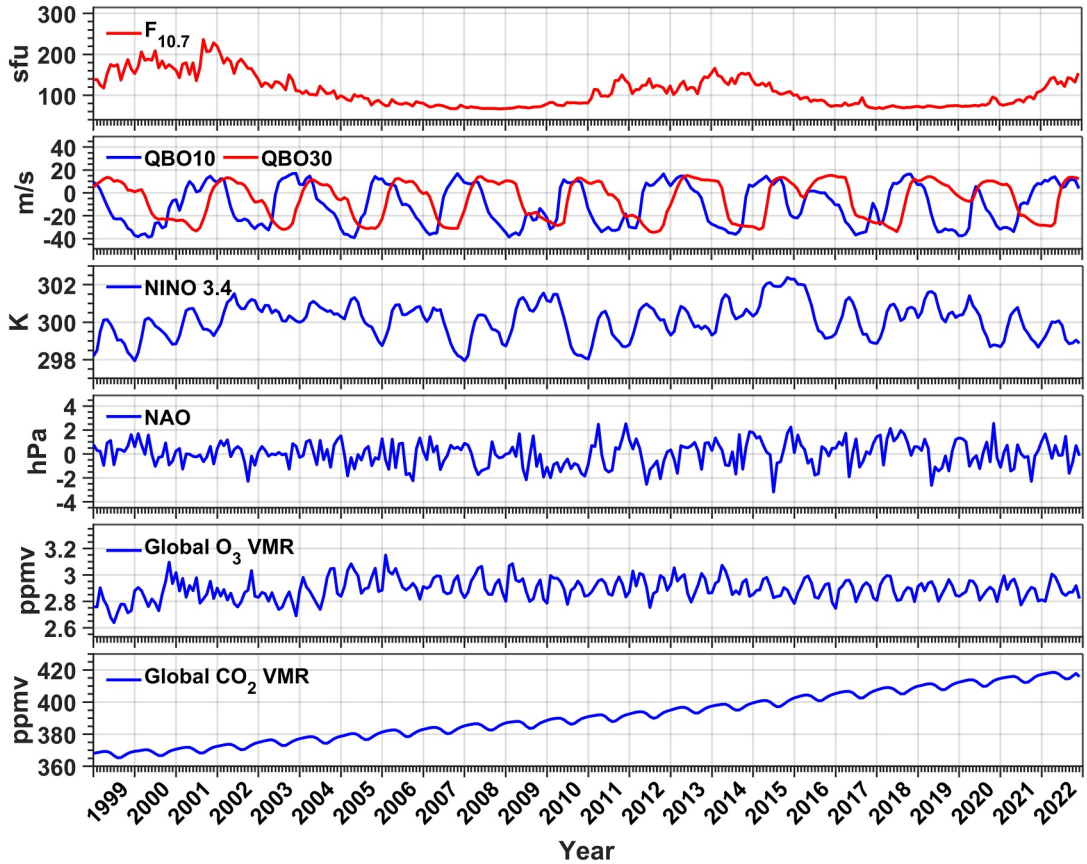

Figure 10. The time series of monthly mean regressors viz., $F_{10.7}$, QBO10, QBO30, NINO 3.4, NAO, O_3, CO_2 for 1999–2022.

1999–2002 and 2011–2015 in consistent with the warm sea surface temperature anomalies, and decreasing trend in recent years signify the reduction in the ENSO variability. The NAO is mostly varying as ±2 hPa and no significant long-term trend is evident in this index. The global mean O_3 VMR at 1 hPa with equinoctial maxima and solstitial minima shows slight increasing trend in the begging years (1999–2001), then declines up to 2003 and again increases until 2005–2006, and then it remains consistent to the end of the observations. The global surface CO_2 VMR obviously shows the increasing trend during the observational period with minima in summer.

The correlation coefficients (r) among the above predictors denote that they are nearly independent as no strong correlation (above $r \sim 0.5$) was observed between them. Furthermore, no multicollinearity exists in the regression analysis and hence the results of the analysis are believed to be more reliable. More details on the r values among these predictors and the multicollinearity check in the MLR analysis can be obtained from Ramesh et al. (2024).

3.5. Zonal and Meridional Semidiurnal Tidal Responses to the Climate Forcings

The monthly anomalies of the amplitudes of zonal and meridional semidiurnal tide calculated with respect to 1999–2003 are subjected to the MLR analysis (defined in Section 2) to investigate their possible responses to the climate forcings at ∼80–100 km in the MLT region.

Figure 11 illustrates the monthly mean anomalies of the zonal tidal amplitudes (ΔU_{12}) along with their responses to the seven potential forcings viz., solar ($F_{10.7}$), QBO10, QBO30, NINO 3.4 (ENSO), NAO, O_3 and CO_2. The stippled regions show the responses which are statistically significant at 90% confidence level from t-test (e.g., Wilks, 2006). From the figure, the regions of the significant response due to the solar forcing are quite less. They can be found as the positive response (∼12 m/s/100 sfu) at higher altitudes above ∼98 km during late autumn (October-November) indicating the tidal enhancement, and the negative response (up to −10 m/s/100 sfu) at ∼85–88 km in the late summer (August) implying the decrease in the tidal amplitudes. The significant negative

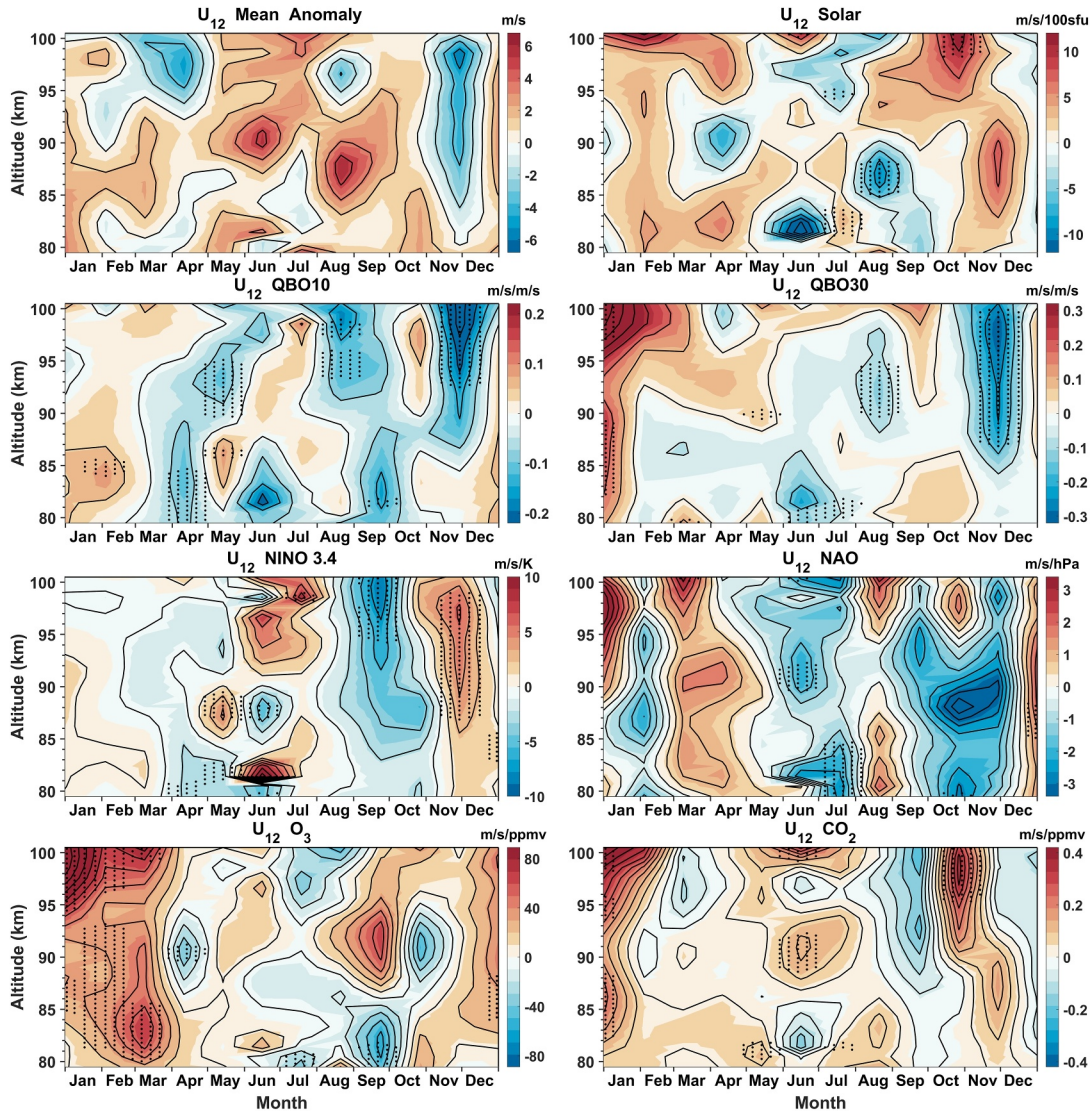

Figure 11. Monthly mean zonal semidiurnal tidal anomalies along with their responses to the seven predictors viz., solar ($F_{10.7}$), QBO10, QBO30, NINO 3.4 (ENSO), NAO, O_3 and CO_2 in the MLT region (~80–100 km) over Esrange. The stippled regions denote the significant responses at 90% confidence level.

responses due to QBO10 and QBO30 in the late autumn/early winter (November–December) above ~85–90 km represent the declining tidal amplitudes. The strong positive response due to QBO30 in the late winter indicate the tidal enhancement, however it is significant in January at ~82–88 km and above ~97 km. Further the significant negative responses due to the QBO (at both the levels) can be found at various heights in spring and summer. The NINO 3.4 index, a proxy for ENSO comprising El Niño or La Niña events, displays the significant negative response above ~95 km in the early autumn indicates the decrease in the tidal amplitude, while the significant positive response above ~85 km in the late autumn/early winter denotes the increase in the tidal amplitude. The response due to NAO is quite variable and mostly insignificant; however, the regions of significant negative responses are limited to summer below ~85 km during July-August and at ~90–92 km in June. The response due to O_3 is significantly positive at almost all the heights during late winter/early spring (January-March), however it is stronger (~80 m/s/ppmv) at higher altitudes above ~95 km in January. This implies that the O_3 likely to amplify the U_{12} during January–March at almost all the heights, with more enhancement (strong amplitudes) in January above ~95 km. The response of U_{12} to CO_2 is significantly positive in late autumn above ~95 km, and at various heights in January and June indicating the enhancement of the tidal amplitude.

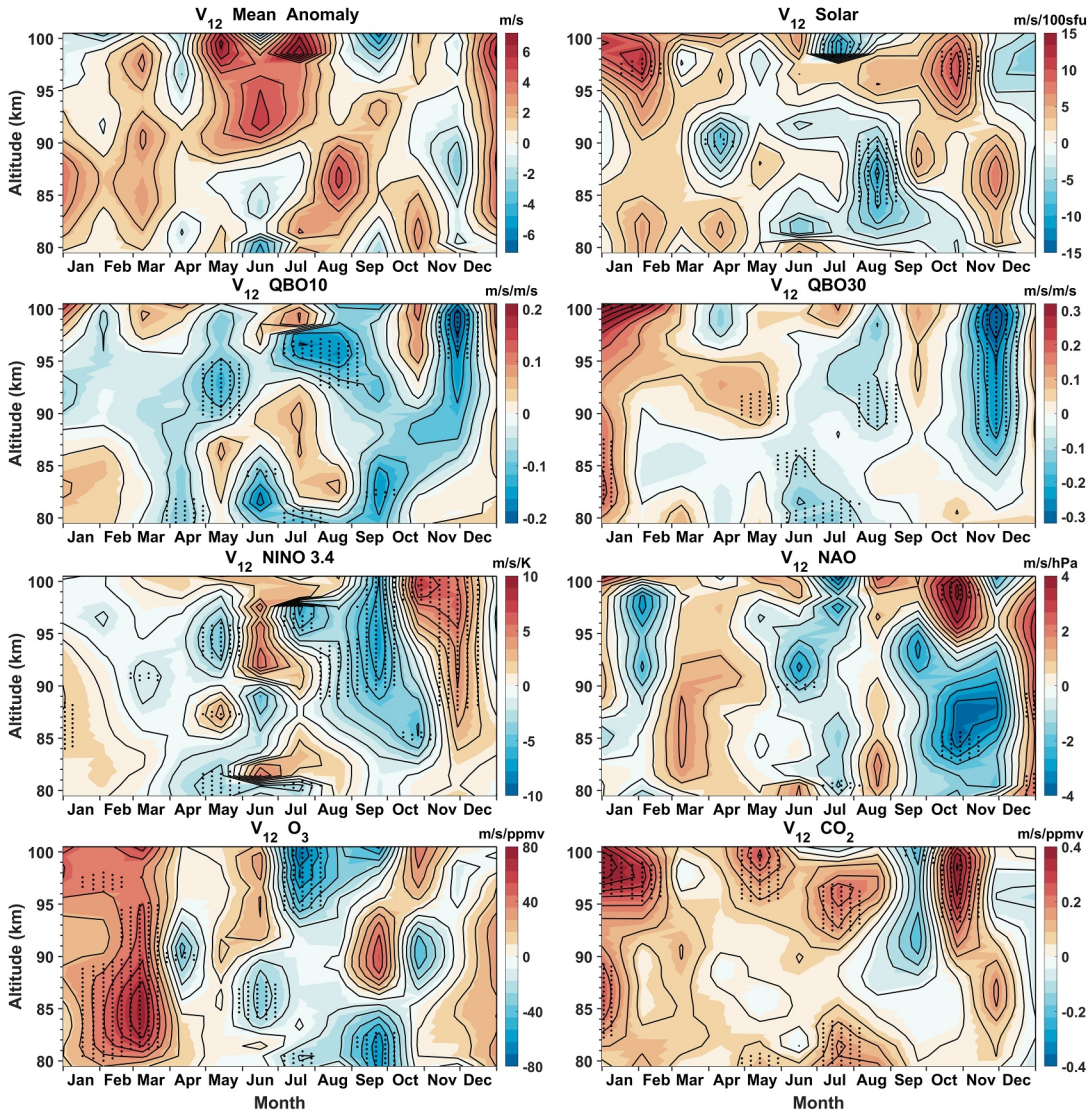

Figure 12. Same as Figure 11 but for meridional semidiurnal tide.

The monthly mean anomalies of the meridional semidiurnal tidal amplitudes (ΔV_{12}) and their responses to the seven predictors are depicted in Figure 12. The stippled regions denote the responses significant at 90% confidence level. Near similar to U_{12}, the meridional tide shows significant positive response to solar forcing (~12 m/s/100 sfu) above ~96 km during late autumn (October–November) implying the enhancement in the tidal amplitude. However, the response is significantly negative (up to −12 m/s/100 sfu) at ~85–90 km in August and above ~98 km during June-July indicating decrease in tidal amplitude. Alike U_{12}, the response of V_{12} to the QBO10 and QBO30 are significantly negative in the late autumn/early winter (November–December) above ~85–90 km implying declining tidal amplitudes. The response due to ENSO (NINO 3.4 index) is significantly negative above ~90 km in the late summer/early autumn, and positive above ~87 km in the late autumn/early winter that denote the decreasing and increasing tidal amplitudes respectively. The response due to NAO is mostly insignificant, however, there are a few regions including significant negative response at around ~85 km and positive response at higher altitudes in late autumn. Like the zonal component, the V_{12} response to O_3 is significantly positive up to ~98 km during late winter/early spring with strong response (~80 m/s/ppmv) centered around ~82–86 km in March. This indicates the O_3 is likely to enhance the amplitude of the meridional tide during late winter/early spring especially with strong impact during February-March below ~90 km. Further the significant negative responses due to O_3 can be found at various heights in summer and below ~85 km in the early

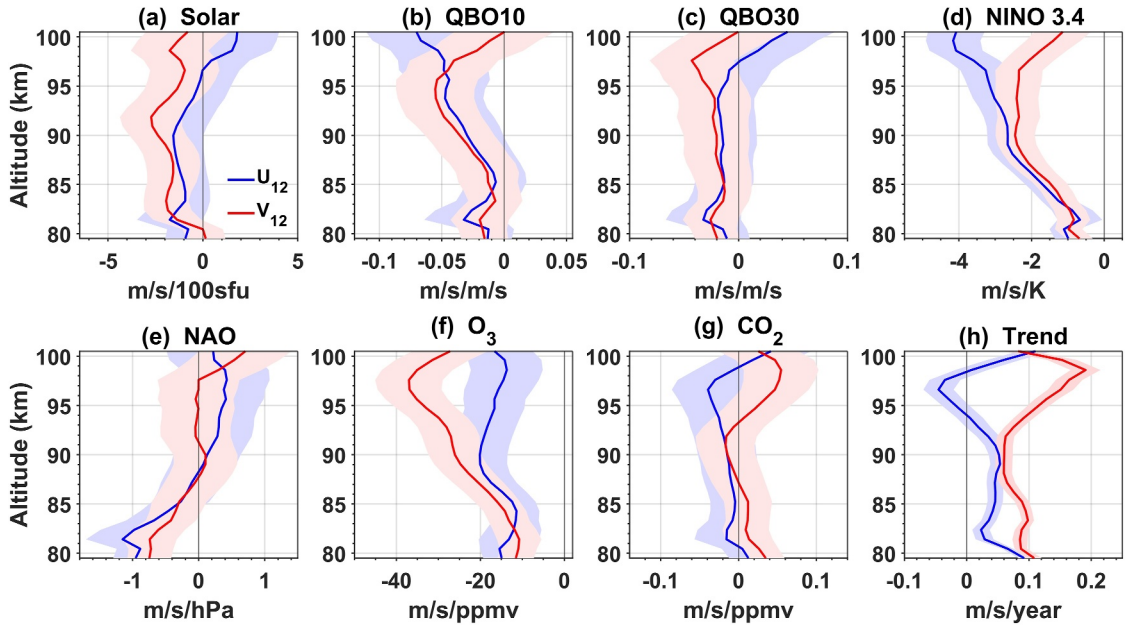

Figure 13. Vertical profiles of cumulative zonal (in blue) and meridional (in red) semidiurnal tidal (a–g) responses to the seven predictors, and (h) trend. The blue and red patches in each panel denote the corresponding standard errors.

autumn, however they are relatively strong (up to −80 m/s/ppmv) above ∼94 km during July–August. The response (significantly positive) of V_{12} to CO_2 is comparable to that of U_{12} in late autumn (October–November), likely to enhance the meridional tidal amplitude above ∼94 km. The strong positive response due to CO_2 can also be found in the late winter (January–February) above ∼95 km and at various heights in late spring/summer.

3.6. Aggregate Responses of the Semidiurnal Tide to Climate Forcings

The cumulative responses of semidiurnal tidal anomalies (ΔU_{12} and ΔV_{12}) to the seven potential drivers viz., solar ($F_{10.7}$), QBO10, QBO30, ENSO (NINO 3.4), NAO, O_3 and CO_2 for all the months and years during 1999–2022 in the MLT region between ∼80 and 100 km are determined from the MLR analysis. Figures 13a–13g shows the altitude variation of the cumulative tidal responses in both components to the above climate forcings. The zonal tidal response to solar forcing is negative, decreases above ∼90 km up to ∼97 km and reverses to positive above this height; however, the meridional tidal response is negative at all the heights. The tidal response to the QBO10 is negative and increases above ∼85 km in both the components; however, the negative response of the meridional tide decreases above ∼95 km. The tidal response to QBO30 remains nearly consistent above ∼85 km in both the components, and the zonal tide response turns to positive above ∼97 km while the negative response of the meridional tide decreases above this height. The response due to ENSO is negative and increases with height for both tidal components, however the negative response of V_{12} decrease above ∼97 km. The tidal response to NAO is negative and decreases with increasing height up to ∼90 km in both the components. Above this height, the response of U_{12} turns to positive, while it is insignificant up to ∼97 km and positively increases above this height for V_{12}. The tidal response to O_3 is negative in both components. In case of U_{12}, it is highly variable with height, decreases below ∼85 km and increases above this height up to ∼90 km. Again, it decreases slightly up to ∼98 km and increases above this height. The negative response of V_{12} increases with height above ∼82 km, peaks at ∼97 km (−35 m/s/ppmv) and decreases above this height. The negative response of U_{12} to CO_2 slightly increases above ∼82 km and decreases beyond ∼97 km to become positive at top altitudes (around ∼99 km). The response of V_{12} is highly variable with altitude, positively decreasing below ∼88 km and negative above this height up to ∼93 km. Again, it turns to positive above this height and increases with altitude peaking at ∼98 km and decreases above this height.

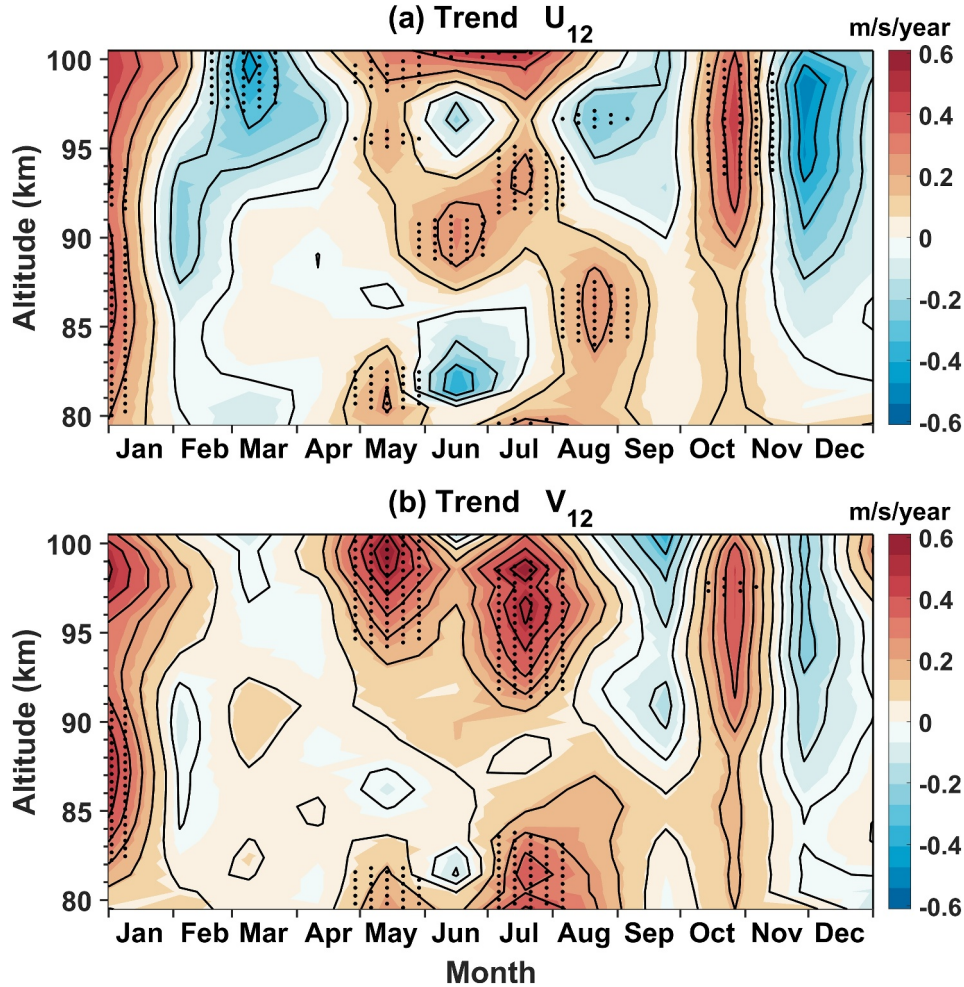

Figure 14. Monthly trends of the (a) zonal, and (b) meridional semidiurnal tide in the MLT region (~80–100 km) during the observational period (1999–2022) over Esrange. The stippled regions denote the significant trends at 90% confidence level.

3.7. Trends in Semidiurnal Tide

The "Trend" here implies changes on a time scale longer than a solar cycle. The altitude variation of cumulative trends in semidiurnal tidal amplitude in both zonal and meridional components are depicted in Figure 13h. The trends are derived as the rate of change of tidal anomalies (ΔU_{12} and ΔV_{12}) for all the months over all the years during 1999–2022. Due to the large correlation between trend (time) and CO_2 index in the MLR analysis, the trends in the tidal amplitudes are calculated irrespective of the climate forcings with no trend term in the regression model (Equation 2). The trend in zonal tide is positive, decreases with increasing height below ~83 km and slightly increases above this height up to ~90 km. The positive trend in U_{12} declines above this height, reverses to negative just below ~95 km and increases to maximum at ~97 km (−0.05 ± 0.02 m/s/year). The trend in U_{12} again becomes positive at around ~98 km and increases with height. The trend in V_{12} is positive at all heights, remains nearly consistent between ~88 and ~92 km. It increases above this height peaking at ~98.5 km (~0.2 ± 0.02 m/s/year) and declines beyond this height.

Figures 14a and 14b illustrates the monthly trends in tidal amplitudes in zonal and meridional components respectively. They represent the rate of change of tidal anomalies for each month over all the years of the observations. The monthly trends are calculated regardless of the climate forcings with no trend (time) term included in the regression model. The significant trends at 90% confidence level are represented by the stippling in the figure panels. The trends in U_{12} are significantly positive (~0.5 m/s/year) above ~92 km during late autumn (October–November) and below ~95 km in the month of January indicating the increasing trend of zonal tidal

amplitude. A few regions of significant positive trends vary with altitude in late spring and summer. However, the trends are significantly negative (−0.5 m/s/year) above ∼97 km in the late winter/early spring representing the decreasing trend in the zonal tidal amplitude. The monthly trends in V_{12} are significantly positive and peaks (∼0.6 m/s/year) above ∼94 km in late spring (May) and at ∼92–98 km in mid-summer (July) suggesting the increasing trend in the meridional tide. The significant positive trends can also be found below ∼84 km during these seasons and further in January between ∼82 and ∼92 km. The positive trends in V_{12} can also be found at the height (above ∼92 km) where the trends in U_{12} are significantly positive in the late autumn, however these trends are mostly insignificant. The negative trends observed above ∼85 km during August–September and November–December are statistically insignificant.

4. Summary and Discussion

In the present study, the meteor radar observations of horizontal winds are used to investigate the long-term variabilities and tendencies of the semidiurnal tide in the northern high latitude MLT during 1999–2022 over Esrange. As the polar (especially Arctic) MLT tidal variabilities are least explored in response to the possible significant drivers, the findings of this study have great importance for comprehensive understanding of the impact of the solar and potential climate forcings (QBO, ENSO, NAO, O_3, and CO_2) on the tidal variabilities in this region. The diurnal variability of the zonal and meridional winds (in 2007) clearly indicates the basic signatures of the 12-hr oscillation (Figures 1 and 2). Further the spectral analysis of the winds at ∼90 km reveals the 24-hr, 12-hr, 8-hr, and 6-hr tidal modes; however, the 12-hr (semidiurnal) tide dominates with largest amplitude in both wind components over Esrange (Figure 3). Hence the present study focuses only on the largest mode, the 12-hr tide to investigate its long-term variabilities and tendencies in response to the above significant climate forcings using the MLR analysis.

The amplitude of the semidiurnal tide increases with height in both the components in the arctic MLT. It is characterized by relatively large amplitude in winter with maximum above ∼95 km and the secondary maximum (with relatively less amplitude) during late summer and early autumn. However, the amplitude of V_{12} is larger than that of U_{12} at higher altitudes. Mitchell et al. (2002) showed the similar seasonal tidal variations using the meteor radar observations for around 1 year (August, 1999–July, 2000) over Esrange. Recently Dutta and Sridharan (2023) also reported the similar seasonal variabilities of the U_{12} and V_{12} amplitudes from the meteor radar observations during 2005–2019 over Esrange. However, Riggin et al. (2003) demonstrated that the tidal (V_{12}) amplitudes maximize around autumnal equinox at ∼86 km in the arctic MLT using the medium frequency (MF) radar observations for 1999–2001 over Andenes (69°N, 16°E) and Poker Flat (65°N, 147°E). They attributed the seasonal enhancement of the semidiurnal tide to reduction in tidal vertical scale in association with refractive effects of wind shears and temperature gradients. However, in the present study, the maximum tidal amplitudes are observed in winter at higher altitudes, even stronger than that in autumnal equinox. The semidiurnal tidal amplitudes are significantly modulated by the nonlinear interaction of migrating tide (SW2) with planetary waves (PWs) and nonmigrating tide. The significant amplification of the PWs in the winter and the nonlinear coupling between the tides and PWs could be the possible reason for the maxima in semidiurnal tidal amplitudes in this season. It can be noted that, as it is not possible to derive the amplitudes of the distinct migrating, nonmigrating tides and PWs with the single location (Esrange) observations, the interaction between these waves cannot be demonstrated here. The winter maxima in semidiurnal tidal amplitudes (Figures 4 and 5) are highly variable (e.g., Pancheva & Mitchell, 2004) and this could be associated with the PW activity and the sudden stratospheric warming (SSW) events (e.g., Chau et al., 2012, 2015; Laskar et al., 2014; Merzlyakov et al., 2001). In spring and summer (Figures 5 and 6), the decrease in the tidal amplitude could be due to the weakening of SW2 and PWs. The least tidal amplitudes in late autumn/early winter could be associated to the combination of out of phase interaction between migrating (SW2) and nonmigrating (SW1) tides, and changes in tidal refractive properties due to changes in other dynamical properties (wind shears and temperature gradients) (e.g., Hibbins et al., 2010; Laskar et al., 2016; Riggin et al., 2003). Pedatella et al. (2021) simulated the SW2 variability and found the pronounced minimum around September equinox in the northern middle and high latitudes. Further they found that the minimum in SW2 tide is due to the seasonal transition of the zonal mean zonal winds which modulate the symmetric and antisymmetric modes of this tide. The enhanced tidal amplitude during August-October could be due to the in-phase interaction between migrating and nonmigrating (SW1) tides (e.g., Laskar et al., 2016).

The interannual variability in the U_{12} and V_{12} amplitudes varies with height (Figure 8) with more pronounced at higher altitudes than at lower altitudes. Further the variability is more obvious when the tidal amplitudes are large especially during winter, and in the late summer and autumn. In the present study, the large tidal amplitudes up to ∼50 m/s are observed (at 98.5 km) in winter of the major SSW years 2001, 2002, 2012, 2013, 2019, 2021. During the minor SSW events of 2000, 2008, 2016, the tidal amplitudes increase moderately up to ∼40 m/s. However, when there is no SSW in 2004 and 2011, no such strong enhancements in the tidal amplitudes are observed. Here it can be noted that, there exist multiple (two or three) SSW events that include major and minor events in different winter months of a single year/season (Zhang & Chen, 2019). The SSW events have substantial impact on the semidiurnal tidal amplitudes in the MLT. They occur primarily due to the interaction of upward propagating PWs of zonal wavenumber 1 or 2 with the zonal mean flow (Matsuno, 1971). The changes in tidal amplitudes are attributed to the changes in zonal winds, changes in tidal sources and nonlinear interactions between the tides and PWs (e.g., Pedatella et al., 2012). It is observed that the winter MLT zonal winds amplify over Esrange during the SSW events (Ramesh et al., 2024). The nonmigrating tide, SW1 can be generated by the nonlinear interaction between the SW2 and the quasi-stationary PW of zonal wavenumber 1 (PW1) (e.g., Liu et al., 2010). The enhancement in SW1 and PW1 (Pedatella et al., 2012) and the interaction between enhanced PW1 and SW2 could significantly increase the semidiurnal tidal amplitude during SSW events. However, Pedatella et al. (2012) simulated that the enhancements in the SW2 is 40%–50% relative to the climatological mean and the changes in the nonmigrating tides are relatively small except the SW1 which shows the changes more than 20% during the SSW events in the northern mid- and high-latitude MLT region. Further it can be observed that there is no enhancement of the tidal amplitude during the major SSW events of 2003 and 2009, possibly associated to the changes in zonal mean zonal winds, ozone forcing and the non-linear interaction of the tides with PWs. In addition, the interaction between enhanced quasi 16-day wave and the semidiurnal tide is maximum around the peak of the major SSWs; however, it is weaker during the minor SSW events (Laskar et al., 2014).

Apart from the above, Hagan et al. (1992) simulated that the variability of the semidiurnal tide (∼5–20 m/s) in the mesosphere could be attributed to the low latitude stratospheric QBO, and it is more pronounced in high latitude winter (January). The interannual variabilities in the tidal amplitudes during August-September could be associated with the behavioral characteristics of the low-latitude QBO. Laskar et al. (2016) found that the tidal amplitudes during August-September enhancement are above and below the mean level for the QBO eastward and westward phases (at 50 hPa) respectively. They hypothesized that the QBO wind modulate the southern hemispheric quasi stationary PW1 (enhance/damp during eastward/westward phases of the QBO) that subsequently interacts with the semidiurnal tide over northern mid-high latitudes to modulate the tidal amplitudes there. Further the interannual variability in U_{12} and V_{12} is also evidenced in summer and autumnal equinox; however, it is more prominent in autumn than in the summer. Smith et al. (2007) analyzed the semidiurnal tidal variability in summer and autumn using the meteor radar observations for 2002–2005 over Esrange. They found that the temporal variability of the semidiurnal tide is well correlated with the PW1 in the stratosphere over southern high latitudes. The correlations suggest that the variability in the tidal amplitude could be due to the dynamical interactions in the opposite (southern) hemisphere.

From the MLR analysis, the tidal responses are robust at the altitude/month where/when the correlations between the tidal anomalies and the predictors are high; however, they are not significant at the areas where no or weak correlations occur as shown in the Figures 11 and 12. The solar forcing plays a significant role to drive the thermal, dynamical processes and their variabilities in the MLT region. In this study, the responses of U_{12} and V_{12} to the solar cycle are found to be significantly positive in late autumn (above ∼95 km) and negative in late summer (at ∼85–90 km) representing the increasing and decreasing tidal amplitudes respectively during solar maximum conditions. Sprenger and Schminder (1969) reported the negative correlation between the solar flux and U_{12} and V_{12} at around 95 km in winter over central Europe (54.1°N, 11.8°E and 51.3°N, 13.0°E). Bremer et al. (1997) found the negative but weak correlation of U_{12}, and almost zero correlation of V12 with the solar activity in most of the months of a year over central Europe. However, from the radar observations, Jacobi et al. (1997) did not find any solar cycle dependence of the semidiurnal tide in most of the months over Collm, Germany (52°N, 15°E). Conversely, Fraser et al. (1989) showed the positive correlation between the solar activity (in the declining phase) and the semidiurnal tidal amplitude in winter over the northern midlatitudes. Though over a southern low-latitude station (22.7oS, 45oW), Guharay et al. (2019) reported the strong positive correlation between U_{12} and the solar activity at the lower heights (below ∼84 km) of the MLT, and negative correlation above this height during the autumnal equinox. They further found that the V_{12} exhibits positive correlation with the solar cycle at all the

observational heights (~80–100 km). In agreement with most of the studies, the present study shows that, the cumulative tidal amplitudes are negatively dependent on the solar cycle at all observational heights except that the U_{12} response reverses to positive above ~97 km (Figure 13). As the nonlinear interaction with PWs plays significant role in the semidiurnal tidal variabilities, the negative response to the solar cycle could be related to the changes in the PW activity (e.g., Baumgaertner et al., 2005). The second mechanism might be the seasonal variations of the stratospheric ozone and strength of the vortex in response to the solar cycle could affect the timing of the large tidal amplitudes in the MLT. Another possible mechanism could be attributed to the changes in pressure and density gradients that affect the tidal vertical propagation and growth. The warming/cooling of the middle atmosphere during increasing/decreasing solar activity in the solar maximum/minimum conditions result in the pressure and density increase/decrease at a given altitude (e.g., Khosravi et al., 2002; Laštovička, 2005). The higher stratospheric temperatures during solar maximum could lead to increased mean densities at the higher altitudes (e.g., Schmidt et al., 2006). The tidal amplitude increases in response to decreasing density with increasing height to conserve the energy and momentum. However, the increase in neutral density during solar maximum could slow down the growth of the tidal amplitudes in the MLT (e.g., Andrioli et al., 2022). This could be the possible reason for the negative tidal response to the solar forcing observed in this study (Figure 13).

The tidal (U_{12} and V_{12}) responses to the QBO at 10 hPa and 30 hPa are significantly negative above ~85–90 km in the late autumn and early winter (Figures 11 and 12). This could be associated to the reduced amplitudes of SW2, SW1 in these seasons. Laskar et al. (2016) suggested that the reduced semidiurnal tidal amplitude after the August-September enhancement period could be due to the out of phase interaction between SW2 and SW1 and changes in refractive properties due to various thermal and dynamical changes. The significant negative tidal responses are also observed at various heights in spring and summer. This maybe associated to the reduced tidal amplitudes due to weakening of SW2 and PWs in these seasons. During winter especially in January, the significant positive response of the semidiurnal tide is observed in both the components. The plausible mechanism could be associated with the tidal modulation due to interaction with the PWs under different phases of the QBO. The QBO modulation of the semidiurnal tide in the northern hemisphere is teleconnected to the PW activity in the opposite hemisphere (Laskar et al., 2016). Hagan et al. (1992) simulated that the effect of stratospheric QBO variability over low latitudes is largely evident on the upward propagating semidiurnal tides (in the wind fields) during January in the high latitude mesosphere. When the QBO winds are eastward, the enhanced PW1 in the southern hemisphere could interact with the SW2 tide in the northern high latitude and enhances the SW1 tide and subsequently the amplitude of the semidiurnal tide in the MLT region. This could be the possible reason for the significant positive responses of the U12 and V12 to the QBO (at 30 hPa) observed in January. The cumulative tidal response to QBO (at 10 hPa and 30 hPa) remains negative (more variable with height for QBO10 than QBO30), except the U12 response to QBO30 above ~97 km where it reverses to positive. The possible reason for the negative tidal responses to QBO could be associated with the dependence of the SSW occurrence on the QBO phase. As stated above, the semidiurnal tidal amplitudes are enhanced during the major SSW events which occur more often under the QBO westward phase than the eastward phase (e.g., Labitzke, 1982; Dunkerton et al., 1988). Therefore, when the QBO phase is eastwards, the occurrence rate of major SSWs is less and thus the reduced tidal amplitudes. Another potential mechanism could be related to the QBO impact on the ozone variability. When the QBO phase is eastward, the weakening of the Brewer-Dobson circulation (due to the QBO induced meridional circulation) (e.g., Andrews et al., 1987) results in the reduced ozone over mid- and high-latitudes. As the semidiurnal tides are excited through the absorption of solar UV radiation by stratospheric ozone, the reduced ozone during the eastward phase of the QBO could result in less tidal forcing. Further the altitude variation of the zonal tidal response to QBO30 mostly resembles with that of the solar forcing (Figures 13a and 13c). This signifies the connection between solar, QBO forcings and the SSW occurrence and their impact on the semidiurnal tidal variability. Salminen et al. (2020) investigated the dependence of the SSW on the internal and external drivers. They found that the effect of the QBO on the occurrence of the SSW strengthens/weakens for the low/high solar (geomagnetic) activity. That is, in QBO westward/eastward phase, the SSWs occur more/less often when the solar (geomagnetic) activity is low/high.

The semidiurnal tide exhibits significant negative response to ENSO in the late summer/early autumn and positive response in the late autumn/early winter above ~85–90 km in both the components. However, the tidal response to ENSO is mostly insignificant in late winter/early spring and significant at various heights in late spring and summer. The large-scale changes in tropospheric convection induced by ENSO could modify the tropospheric tidal forcing (Lieberman et al., 2007; Trenberth et al., 2002). Depending on the specific tide, the

increase or decrease in the tidal forcing in response to ENSO results in changes in the tidal amplitudes in the MLT (e.g., Gurubaran et al., 2005; Lieberman et al., 2007). Hagan and Forbes (2003) simulated that the semidiurnal tide in the MLT is influenced by latent heat release associated with raindrop formation in tropospheric deep convective clouds over the tropics. They further illustrated that the year-to-year variability in the tropospheric tidal forcing of the semidiurnal tide can be expected in association with deep convective activity over the tropics. However, the monthly variations in the tidal responses could be possibly due to ENSO induced changes in the tropospheric precipitation change slowly over several months (e.g., Trenberth et al., 2002). In addition, the changes in stratospheric and mesospheric zonal winds in response to ENSO could be another source of tidal variability in the MLT (Sassi et al., 2004). Ramesh et al. (2024) found significant positive response of the zonal winds to ENSO during late autumn/early winter, and negative response of the meridional winds in summer/early autumn below ∼90–95 km over Esrange. In the present study, the significant tidal responses to ENSO are found above this height. This indicates the tidal variability in response to ENSO can also result from the wind variations due to ENSO in the MLT. Furthermore, Pedatella and Liu. (2012) suggested that the changes in PW activity due to ENSO can influence the zonal mean winds, resulting in additional modulation of the tides in the MLT. Besides, in the present study, the significant opposite responses due to ENSO (positive) and QBO (negative) observed in both components of the semidiurnal tide during late autumn/early winter (above ∼85–90 km) indicating the relationship between these two dominant modes of climate variability. That is, the hydrostatic effects of QBO linked zonal wind shear likely to enhance/suppress the equatorial deep convective activity during westward/eastward phase of the QBO (Gray et al., 1992). The cumulative tidal response to ENSO is negative in both components at all observational heights (Figure 13d). This could be possibly due to the response of the tide especially the nonmigrating components to the El Niño and La Niña phases of the ENSO. Warner and Oberheide (2014) found the larger radiative heating occur during La Niña phase than the El Niño phase and most of the heating occurs in the southern hemisphere. However, the larger heating in the southern hemisphere during La Niña occurs along with the larger tidal amplitudes in the northern hemisphere, and it could be because of the global nature of the tides combined with phase interference (Warner & Oberheide, 2014).

The tidal response to NAO is mostly insignificant except at some parts in summer, autumn, and early winter. In winter when the NAO is more pronounced (NAO index is high), the positive tidal response to the NAO is found in December, but at very limited heights. In summer when the NAO is weak (NAO index is low), the tidal responses are negative but significant at limited heights especially during June-July (Figures 11 and 12). According to Jacobi and Beckmann., (1999), in winter, the polar vortex is directly dynamically coupled to the troposphere and the MLT and thus the NAO index can be correlated to the dynamical parameters from both the regions of the atmosphere. However, in summer, the dynamical coupling could be weaker when the stratospheric westward winds prevent westward traveling PWs from propagating into the MLT. In addition, the tidal amplitudes are relatively larger in winter (above ∼85 km) and smaller in summer. The opposite responses of V_{12} to the NAO (negative below and positive above ∼90–95 km) are observed during September–November, however, they are insignificant in case of U_{12}. The cumulative tidal responses to NAO are negative below∼88 km and reverse to positive above this height; however, the V_{12} response is insignificant at ∼92–98 km. This behavior can be expected due to the height variation of the tidal amplitude especially during and after the August-October maximum, wave modulation by background winds, and non-linear wave-wave (tides, GWs and PWs) interactions during strong (positive) and weak (negative) NAO (index). The long-term responses of MLT winds to NAO over Esrange can be found in Ramesh et al. (2024).

The semidiurnal tidal response to ozone is positive in winter/early spring with strong and significant responses during January–March in both the components (Figures 11 and 12). This could be associated mostly to the SSW induced changes in the ozone, and thus the amplitudes of the semidiurnal tide. As the SSWs are large scale transient events in the winter polar stratosphere, any changes in dynamical and chemical processes before, during and after the SSW events could profoundly impact the chemical composition including ozone in the polar middle atmosphere (e.g., Sofieva et al., 2012). However, the changes in stratospheric ozone during SSWs are strongly dependent on altitude (e.g., de la Cámara et al., 2018) with which the dynamical (lower stratosphere) and chemical (upper stratosphere) processes change. The PW breaking accompanying the onset of an SSW accelerates the Brewer-Dobson circulation (McIntyre, 1982) leading to warming of the stratosphere. Additionally, the downward transport of NOx is terminated, preventing the O_3 losses through the chemical reactions with NOx, while the primary source of O_3 remains unchanged (Denton et al., 2019). These processes combinedly lead to a rapid increase in O_3 levels in the upper stratosphere and mesosphere immediately after an SSW event. As the absorption

of solar UV radiation by ozone is the primary source for the generation of SW2 tide (e.g., Forbes & Garrett, 1978; Lindzen & Chapman, 1969), the increase in ozone density could result in the enhancement of this tide during SSWs (e.g., Siddiqui et al., 2019). However, Pedatella et al. (2014) simulated that the SW2 changes were driven by the combination of changes in the zonal mean zonal winds and the changes in stratospheric ozone during the 2009 SSW event. Goncharenko et al. (2012) reported that, during the 2009 major SSW event, PW forcing induced large-scale global circulation changes led to the enhancement of the ozone density by 25% in the tropical stratosphere (30–50 km) where the SW2 tide is primarily generated. Further they suggested that the stratospheric circulation changes during SSW can increase the longitudinal inhomogeneities in the distribution of the ozone that can result in the generation of the nonmigrating tides. Sridharan et al. (2012) found the increase in the semidiurnal tidal amplitudes in the tropical mesosphere during major SSW events of 2006 and 2009; they linked it to the enhancement of the tropical stratospheric ozone due the weakening of the Brewer Dobson circulation during SSWs. The variations in the nonmigrating tides (SW1 and SW3) could be due to the nonlinear interaction between the enhanced PWs and the migrating tide (SW2) during SSWs (e.g., Liu et al., 2010; Pedatella & Forbes, 2010). On the other hand, Sridharan et al. (2012) reported an unusual reduction in the mesospheric semidiurnal tide over the tropics (8.7°N, 77.8°E) prior to the onset of a minor stratospheric warming event in 2011. They suggested that the enhanced PW activity prior to the occurrence of the 2011 minor SSW strengthened the Brewer-Dobson circulation which transports stratospheric O_3 to the northern high latitudes. Therefore, in the present study, the positive tidal responses to the ozone in the winter/early spring could possibly be attributed to the above dynamical and chemical processes during major and minor SSW events. In addition, the negative tidal responses to ozone in summer/early autumn could be associated with less ozone due to weak eddy mixing and/or other dynamical and chemical processes, less PW activity, and thus weaker tidal amplitudes. However, the cumulative tidal responses to ozone are negative at all observational heights with a maximum V_{12} response at around ∼97 km. This could be possibly associated with, in addition to the above, the response of the ozone and semidiurnal tide to the solar flux variations, and the variability of the V12 is slightly strongly dependent on the solar activity than that of U_{12} (e.g., Pancheva et al., 2003).

The tidal responses to CO_2 are significantly positive in mid-late winter, and during mid-late autumn at higher altitudes above ∼95 km. Significant positive responses can also be found at various heights in late spring/summer in both the tidal components. Further the tidal responses to CO_2 are nearly identical to that of ENSO especially during the autumnal equinox when the El Niño intensity tends to maximize (Figures 11 and 12). The semidiurnal tide can be excited by large-scale latent heat release due to deep convection in the troposphere (Forbes et al., 1997; Hagan & Forbes, 2003; Lindzen, 1978). The global warming due to rising levels of CO_2 could lead to more frequent and intense El Niño events (e.g., Cai et al., 2022), and thus influence the tropical deep convective systems and tidal forcings, subsequently the semidiurnal tidal amplitudes in the MLT region. On the other hand, it is evidenced that there exist correlations between the atmospheric CO_2 growth rate and El Niño activity (Betts et al., 2016; Chatterjee et al., 2017 and references therein), that is, the global atmospheric CO_2 increases during El Niño events. However, during La Niña events the annual CO_2 growth rate is slower. The impact of El Niño and La Niña is very small in summer, and this could be the possible reason for relatively weak positive tidal responses to CO_2 in this season. The positive tidal response to CO_2 in January-February could be attributed to increasing number of SSWS due to increasing CO_2 (e.g., Schimanke et al., 2013). The cumulative tidal response to CO_2 varies with altitude, with maximum negative and positive responses of U_{12} and V_{12} occur at around ∼97–99 km. However, the U_{12} response reverses to positive above this height. The rising levels of CO_2 lead to infrared cooling which could result in reduced tidal dissipation due to weaker heat conduction and molecular viscosity at higher levels of the MLT (e.g., Sun et al., 2022). The positive tidal responses to CO_2 represent the increasing tidal amplitudes likely due to decreasing wave dissipation associated to the radiative cooling at higher altitudes.

The significant positive trends in the tidal amplitudes in late spring/summer and mid-winter (January) at various heights implies the increasing trends in the tidal amplitudes with relatively strong trends in the meridional component. Above 90 km, the positive trends in V_{12} are maximum (∼0.6 m/s/year) in May and July. This could be probably associated to the trends in meridional wind. Ramesh et al. (2024) showed a strengthening of the summer to winter pole meridional circulation over Esrange, mostly in response to the increasing CO_2. In addition, the increasing radiative cooling in the summer polar mesosphere due to increasing greenhouse gases (GHGs) (e.g., Bailey et al., 2021) could lead to weaker heat conduction and molecular viscosity which in turn could result in decreasing tidal dissipation, and hence the increasing trend in the tidal amplitudes. The significant increasing trend in the tidal amplitudes in mid-winter can be attributed to the complex processes associated to the SSWs.

From ensemble simulations, Schimanke et al. (2013) reported an increase in the number of SSWs from the pre-industrial period to the end of 21st century predominantly due to increasing GHGs. Further they simulated that the intensity of the SSWs is moderately reduced due to increase in GHGs. In the present study, the significant positive trends in the tidal amplitudes in January month could be associated to increasing frequency of SSWs in association with increasing GHGs. The cumulative trend in the zonal tide is positive below ∼95 km, it reverses to negative above this height peaking at ∼97 km, and again turns to positive above this height (Figure 13h). However, the trend in meridional tide is positive at all observational heights with maximum at ∼98 km, and it decreases above this height. The trends in the tidal amplitudes are likely associated to increasing CO_2 that significantly influence (through cooling effect) the tidal amplitudes especially at higher altitudes; however, they can vary depending on the month/season for the zonal and meridional components of the tide. The positive trends in the tidal amplitudes could be due to increase in the SW2 tidal forcing associated to the stratospheric ozone enhancement by the increasing CO_2 radiative cooling (e.g., Liu et al., 2020). Further, the negative trend in pressure altitude (decreasing altitude for a given pressure level) due to the middle atmosphere CO_2 cooling (e.g., Bailey et al., 2021; Zhao et al., 2020) could lead to the positive trends in the semidiurnal tidal amplitudes.

5. Conclusions

The long-term, interannual variabilities and tendencies of the monthly zonal and meridional semidiurnal tide in the northern polar MLT are derived from the meteor radar observations at ∼80–100 km during 1999–2022 (two SCs) over Esrange (67.9°N, 21.1°E). In addition, for the first time, the broad impact of the potential climate forcings viz., SC, QBO (at 10 and 30 hPa), ENSO, NAO, O_3, and CO_2 on the arctic MLT semidiurnal tide has been investigated using MLR analysis for the observational period.

The important conclusions of this study can be listed as follows.

1. The spectral analyses of zonal and meridional winds reveal the dominance of the semidiurnal (12-hr) tide over the diurnal (24-hr) and terdiurnal (8-hr) tide in the arctic MLT (at ∼90 km) during 1999–2022 over Esrange.
2. The climatological means of the semidiurnal tidal amplitude in both components are significantly large at higher altitudes (above ∼90–95 km) in winter and late summer/early autumn (August–September).
3. The monthly mean U_{12} and V_{12} amplitudes exhibit significant interannual variability that changes with altitude and month or season. The variability is more pronounced during autumn and winter, and smaller in summer at 89.9 and 98.5 km.
4. The U_{12} and V_{12} responses to solar forcing are significantly positive at higher altitudes (above ∼98 km) in the late autumn and negative at ∼85–88 km in late summer. The positive/negative responses due to solar forcing represent the increase/decrease in tidal amplitudes during solar maximum conditions.
5. The significant negative tidal responses to QBO (at 10 hPa and 30 hPa) above ∼85–90 km in the late autumn/early winter indicates the decreasing tidal amplitude during eastward phase of the QBO.
6. The significant negative response of U_{12} and V_{12} to ENSO during autumnal equinox above ∼95 km indicates the decrease in the tidal amplitude, while the significant positive response above ∼85 km in the late autumn/early winter denotes the increase in the tidal amplitude during the El Niño events.
7. The tidal response to NAO is mostly insignificant except in summer (negative) at various heights, and at around ∼85 km during mid-late autumn for V_{12}.
8. The significant positive responses of U_{12} and V_{12} to O_3 during January-March represent the increase in tidal amplitudes likely due to the SSWs induced changes in ozone concentrations.
9. The responses of U_{12} and V_{12} to CO_2 are significantly positive in late autumn above ∼95 km, and at various heights in January and June imply the enhancement of the tidal amplitude likely due to the consequences of increasing CO_2.
10. The positive trends of V_{12} are significantly larger than that of U_{12} especially above ∼90 km in late spring/summer.

Data Availability Statement

The Esrange meteor radar data used in this study can be obtained from the UK Centre for Environmental Data Archival (CEDA), Mitchell (2019) for 2000–2018, and from Genesis software Ltd. (https://www.gsoft.com.au/)

for the remaining years upon request. The monthly $F_{10.7}$ values are from Laboratory for Atmospheric and Space Physics (2005). The QBO indices (at 10 and 30 hPa) and the O_3 mass mixing ratio (MMR) are obtained from ERA5 reanalysis, Hersbach et al. (2023). The O3 MMR is converted to its VMR as per Ramesh et al. (2024). The monthly NINO 3.4 index data are provided by NOAA/PSL and can be obtained from National Oceanic and Atmospheric Administration (2023c). The monthly NAO index values are provided by NOAA/CPC and can be obtained from National Oceanic and Atmospheric Administration (2023a). The monthly CO2 VMR data is provided by NOAA/GML and can be obtained from National Oceanic and Atmospheric Administration (2023b).

Acknowledgments
KR, TMG, and NJM are funded through the MesoS2D (Mesospheric sub-Seasonal to Decadal predictability) by UK Natural Environment Research Council (NERC Grant Reference: NE/V018426/1) for this work. NPH is supported by NERC Grants NE/X017842/1, NE/W003201/1, and NE/S00985X/1. The Esrange meteor radar is operated and maintained by Esrange Space Center, Swedish Space Corporation (SSC) since October 2015. Previously, it was operated by University of Bath, UK. The authors thank the editor and two anonymous reviewers for their constructive and insightful comments which improvise the manuscript.

References

Achatz, U., Grieger, N., & Schmidt, H. (2008). Mechanisms controlling the diurnal solar tide: Analysis using a GCM and a linear model. *Journal of Geophysical Research*, *113*(A8), A08303. https://doi.org/10.1029/2007JA012967

Akmaev, R. A., Fuller-Rowell, T. J., Wu, F., Forbes, J. M., Zhang, X., Anghel, A. F., et al. (2008). Tidal variability in the lower thermosphere: Comparison of Whole Atmosphere Model (WAM) simulations with observations from TIMED. *Geophysical Research Letters*, *35*(3), L03810. https://doi.org/10.1029/2007GL032584

Andrews, D. G., Holton, J. R., & Leovy, C. B. (1987). *Middle atmosphere dynamics*. Academic Press.

Andrioli, V. F., Xu, J., Batista, P. P., Resende, L. C. A., Da Silva, L. A., Marchezi, J. P., et al. (2022). New findings relating tidal variability and solar activity in the low latitude MLT region. *Journal of Geophysical Research: Space Physics*, *127*(3), e2021JA030239. https://doi.org/10.1029/2021JA030239

Arras, C., Jacobi, C., & Wickert, J. (2009). Semidiurnal tidal signature in sporadic E occurrence rates derived from GPS radio occultation measurements at higher midlatitudes. *Annales Geophysicae*, *27*(6), 2555–2563. https://doi.org/10.5194/angeo-27-2555-2009

Bailey, S. M., Thurairajah, B., Hervig, M. E., Siskind, D. E., Russell, J. M., & Gordley, L. L. (2021). Trends in the polar summer mesosphere temperature and pressure altitude from satellite observations. *Journal of Atmospheric and Solar-Terrestrial Physics*, *220*, 105650. https://doi.org/10.1016/j.jastp.2021.105650

Baumgaertner, A. J. G., McDonald, A. J., Fraser, G. J., & Plank, G. E. (2005). Long-term observations of mean winds and tides in the upper mesosphere and lower thermosphere above Scott Base, Antarctica. *Journal of Atmospheric and Solar-Terrestrial Physics*, *67*(16), 1480–1496. https://doi.org/10.1016/j.jastp.2005.07.018

Betts, R., Jones, C., Knight, J., Keeling, R. F., & Kennedy, J. J. (2016). El Niño and a record CO_2 rise. *Nature Climate Change*, *6*(9), 806–810. https://doi.org/10.1038/nclimate3063

Bremer, J., Schminder, R., Greisiger, K. M., Hoffmann, P., Kürschner, D., & Singer, W. (1997). Solar cycle dependence and long-term trends in the wind field of the mesosphere/lower thermosphere. *Journal of Atmospheric and Solar-Terrestrial Physics*, *59*(5), 497–509. https://doi.org/10.1016/S1364-6826(96)00032-6

Cai, W., Ng, B., Wang, G., Santoso, A., Wu, L., & Yang, K. (2022). Increased ENSO Sea surface temperature variability under four IPCC emission scenarios. *Nature Climate Change*, *12*(3), 228–231. https://doi.org/10.1038/s41558-022-01282-z

Chang, L., Palo, S., Hagan, M., Richter, J., Garcia, R., Riggin, D., & Fritts, D. (2008). Structure of the migrating diurnal tide in the whole atmosphere community model (WACCM). *Advances in Space Research*, *41*(9), 1398–1407. https://doi.org/10.1016/j.asr.2007.03.035

Chapman, S., & Lindzen, R. S. (1970). *Atmospheric tides*. D. Reidel.

Chatterjee, A., Gierach, M. M., Sutton, A. J., Feely, R. A., Crisp, D., Eldering, A., et al. (2017). Influence of El Niño on atmospheric CO_2 over the tropical Pacific Ocean: Findings from NASA's OCO-2 mission. *Science*, *358*(6360), eaam5776. https://doi.org/10.1126/science.aam5776

Chau, J. L., Goncharenko, L. P., Fejer, B. G., & Liu, H.-L. (2012). Equatorial and low latitude ionospheric effects during sudden stratospheric warming events. *Space Science Reviews*, *168*(1–4), 385–417. https://doi.org/10.1007/s11214-011-9797-5

Chau, J. L., Hoffmann, P., Pedatella, N. M., Matthias, V., & Stober, G. (2015). Upper mesospheric lunar tides over middle and high latitudes during sudden stratospheric warming events. *Journal of Geophysical Research: Space Physics*, *120*(4), 3084–3096. https://doi.org/10.1002/2015ja020998

Covey, C., Dai, A., Lindzen, R. S., & Marsh, D. R. (2014). Atmospheric tides in the latest generation of climate models. *Journal of the Atmospheric Sciences*, *71*(6), 1905–1913. https://doi.org/10.1175/JAS-D-13-0358.1

de la Cámara, A., Abalos, M., Hitchcock, P., Calvo, N., & Garcia, R. R. (2018). Response of Arctic ozone to sudden stratospheric warmings. *Atmospheric Chemistry and Physics*, *18*(22), 16499–16513. https://doi.org/10.5194/acp-18-16499-2018

Dempsey, S. M., Noble, P. E., Wright, C. J., Mitchell, N. J., & Moffat-Griffin, T. (2022). Interannual variability of the 12-hr tide in the mesosphere and lower thermosphere in 15 years of meteor-radar observations over Rothera (68°S, 68°W). *Journal of Geophysical Research: Atmospheres*, *127*(22), e2022JD036694. https://doi.org/10.1029/2022JD036694

Denton, M., Kivi, R., Ulich, T., Rodger, C., Clilverd, M., Denton, J., & Lester, M. (2019). Observed response of stratospheric and mesospheric composition to sudden stratospheric warmings. *Journal of Atmospheric and Solar-Terrestrial Physics*, *191*, 105054. https://doi.org/10.1016/j.jastp.2019.06.001

Dunkerton, T. J., Delisi, D. P., & Baldwin, M. P. (1988). Distribution of major stratospheric warmings in relation to the quasi-biennial oscillation. *Geophysical Research Letters*, *15*(2), 136–139. https://doi.org/10.1029/GL015i002p00136

Dutta, R., & Sridharan, S. (2023). Observational evidence for the influence of diurnal tide in driving winds in the polar upper mesosphere and lower thermosphere. *Journal of Geophysical Research: Space Physics*, *128*(3), e2022JA031104. https://doi.org/10.1029/2022JA031104

Fiedler, J., & Baumgarten, G. (2018). Solar and lunar tides in noctilucent clouds as determined by ground-based lidar. *Atmospheric Chemistry and Physics*, *18*(21), 16051–16061. https://doi.org/10.5194/acp-18-16051-2018

Forbes, J. M. (1995). Tidal and planetary waves. In *The Upper Mesosphere and Lower Thermosphere: A Review of Experiment and Theory*. In *Geophysical Monograph Series* (pp. 67–87). AGU.

Forbes, J. M., & Garrett, H. B. (1978). Thermal excitation of atmospheric tides due to insolation absorption by O_3 and H_2O. *Geophysical Research Letters*, *5*(12), 1013–1016. https://doi.org/10.1029/GL005i012p01013

Forbes, J. M., Hagan, M. E., & Zhang, X. (2007). Seasonal cycle of nonmigrating diurnal tides in the MLT region due to tropospheric heating rates from the NCEP/NCAR Reanalysis Project. *Advances in Space Research*, *39*(8), 1347–1350. https://doi.org/10.1016/j.asr.2003.09.076

Forbes, J. M., Hagan, M. E., Zhang, X., & Hamilton, K. (1997). Upper atmosphere tidal oscillations due to latent heat release in the tropical troposphere. *Annales Geophysicae*, *15*(9), 1165–1175. https://doi.org/10.1007/s00585-997-1165-0

Forbes, J. M., Zhang, X., Palo, S., Russell, J., Mertens, C. J., & Mlynczak, M. (2008). Tidal variability in the ionospheric dynamo region. *Journal of Geophysical Research*, *113*(A2), A02310. https://doi.org/10.1029/2007JA012737

Fraser, G. J., Vincent, R. A., Manson, A. H., Meek, C. E., & Clark, R. R. (1989). Inter-annual variability of tides in the mesosphere and lower thermosphere. *Journal of Atmospheric and Terrestrial Physics*, *51*(7–8), 555–567. https://doi.org/10.1016/0021-9169(89)90054-8

Fritts, D. C., & Alexander, M. J. (2003). Gravity wave dynamics and effects in the middle atmosphere. *Reviews of Geophysics*, *41*, 1003. https://doi.org/10.1029/2001RG000106

Fritts, D. C., & Vincent, R. A. (1987). Mesospheric momentum flux studies at Adelaide, Australia: Observations and a gravity wave–tidal interaction model. *Journal of the Atmospheric Sciences*, *44*(3), 605–619. https://doi.org/10.1175/1520-0469(1987)044<0605:MMFSAA>2.0.CO;2

Gan, Q., Du, J., Ward, W. E., Beagley, S. R., Fomichev, V. I., & Zhang, S. (2014). Climatology of the diurnal tides from eCMAM30 (1979 to 2010) and its comparison with SABER. *Earth Planets and Space*, *66*(1), 103. https://doi.org/10.1186/1880-5981-66-103

Goncharenko, L., Liu, H.-L., Chau, J., Stober, G., Sunkara, E., & Zabotin, N. (2023). Importance of the semidiurnal tide, and future measurements needed to improve its characterization. *Bulletin of the AAS*, *55*(3). https://doi.org/10.3847/25c2cfeb.8afcb212

Goncharenko, L. P., Coster, A. J., Plumb, R. A., & Domeisen, D. I. V. (2012). The potential role of stratospheric ozone in the stratosphere-ionosphere coupling during stratospheric warmings. *Geophysical Research Letters*, *39*(8), L08101. https://doi.org/10.1029/2012GL051261

Gray, W. M., Sheaffer, J. D., & Knaff, J. A. (1992). Influence of the stratospheric QBO on ENSO variability. *Journal of the Meteorological Society of Japan*, *70*(5), 975–995. https://doi.org/10.2151/jmsj1965.70.5_975

Grieger, N., Volodin, E. M., Schmitz, G., Hoffmann, P., Manson, A. H., Fritts, D. C., et al. (2002). General Circulation Model results on migrating and nonmigrating tides in the mesosphere and lower thermosphere. Part 1: Comparison with observations. *Journal of Atmospheric and Solar-Terrestrial Physics*, *64*(8–11), 897–911. https://doi.org/10.1016/s1364-6826(02)00045-7

Guharay, A., Batista, P., & Andrioli, V. (2019). Investigation of solar cycle dependence of the tides in the low latitude MLT using meteor radar observations. *Journal of Atmospheric and Solar-Terrestrial Physics*, *193*, 105083. https://doi.org/10.1016/j.jastp.2019.105083

Gurubaran, S., & Rajaram, R. (1999). Long-term variability in the mesospheric tidal winds observed by MF radar over Tirunelveli (8.7°N, 77.8°E). *Geophysical Research Letters*, *26*(8), 1113–1116. https://doi.org/10.1029/1999GL900171

Gurubaran, S., Rajaram, R., Nakamura, T., & Tsuda, T. (2005). Interannual variability of diurnal tide in the tropical mesopause region: A signature of the El Nino-Southern Oscillation (ENSO). *Geophysical Research Letters*, *32*(13), L13805. https://doi.org/10.1029/2005GL022928

Hagan, M., Forbes, J., & Vial, F. (1995). On modeling migrating solar tides. *Geophysical Research Letters*, *22*(8), 893–896. https://doi.org/10.1029/95GL00783

Hagan, M. E., Burrage, M. D., Forbes, J. M., Hackney, J., Randel, W. J., & Zhang, X. (1999). GSWM-98: Results for migrating solar tides. *Journal of Geophysical Research*, *104*(A4), 6813–6828. https://doi.org/10.1029/1998ja900125

Hagan, M. E., & Forbes, J. M. (2002). Migrating and nonmigrating diurnal tides in the middle and upper atmosphere excited by tropospheric latent heat release. *Journal of Geophysical Research*, *107*(D24), 4754. https://doi.org/10.1029/2001JD001236

Hagan, M. E., & Forbes, J. M. (2003). Migrating and nonmigrating semidiurnal tides in the upper atmosphere excited by tropospheric latent heat release. *Journal of Geophysical Research*, *108*, 1062. https://doi.org/10.1029/2002JA009466

Hagan, M. E., Roble, R. G., & Hackney, J. (2001). Migrating thermospheric tides. *Journal of Geophysical Research*, *106*(A7), 12739–12752. https://doi.org/10.1029/2000JA000344

Hagan, M. E., Vial, F., & Forbes, J. M. (1992). Variability in the upward propagating semidiurnal tide due to effects of QBO in the lower atmosphere. *Journal of Atmospheric and Terrestrial Physics*, *54*(11), 1465–1474. https://doi.org/10.1016/0021-9169(92)90153-C

Hersbach, H., Bell, B., Berrisford, P., Biavati, G., Horányi, A., Muñoz Sabater, J., et al. (2023). ERA5 hourly data on pressure levels from 1940 to present [Dataset]. *Copernicus Climate Change Service (C3S) Climate Data Store (CDS)*. https://doi.org/10.24381/cds.bd0915c6

Hibbins, R. E., Espy, P. J., & Jarvis, M. J. (2007). Quasi-biennial modulation of the semidiurnal tide in the upper mesosphere above Halley, Antarctica. *Geophysical Research Letters*, *34*(21), L21804. https://doi.org/10.1029/2007GL031282

Hibbins, R. E., Marsh, O. J., McDonald, A. J., & Jarvis, M. J. (2010). A new perspective on the longitudinal variability of the semidiurnal tide. *Geophysical Research Letters*, *37*(14), L14804. https://doi.org/10.1029/2010GL044015

Hindley, N. P., Mitchell, N. J., Cobbett, N., Smith, A. K., Fritts, D. C., Janches, D., et al. (2022). Radar observations of winds, waves and tides in the mesosphere and lower thermosphere over South Georgia island (54°S, 36°W) and comparison with WACCM simulations. *Atmospheric Chemistry and Physics*, *22*(14), 9435–9459. https://doi.org/10.5194/acp-22-9435-2022

Hocking, W., Fuller, B., & Vandepeer, B. (2001). Real-time determination of meteor-related parameters utilizing modern digital technology. *Journal of Atmospheric and Solar-Terrestrial Physics*, *63*(2–3), 155–169. https://doi.org/10.1016/s1364-6826(00)00138-3

Jacobi, C., & Beckmann, B. R. (1999). On the connection between upper atmospheric dynamics and tropospheric parameters: Correlations between mesopause region winds and the North Atlantic oscillation. *Climatic Change*, *43*(3), 629–643. https://doi.org/10.1023/A:1005451227975

Jacobi, C., Schminder, R., Kürschner, D., Bremer, J., Greisiger, K., Hoffmann, P., & Singer, W. (1997). Long-term trends in the mesopause wind field obtained from LF D1 wind measurements at Collm, Germany. *Advances in Space Research*, *20*(11), 2085–2088. https://doi.org/10.1016/S0273-1177(97)00599-1

Kato, S., Tsuda, T., & Wantanabe, F. (1982). Thermal excitation of non-migrating tides. *Journal of Atmospheric and Terrestrial Physics*, *44*(2), 131–146. https://doi.org/10.1016/0021-9169(82)90116-7

Khosravi, R., Brasseur, G., Smith, A., Rusch, D., Walters, S., Chabrillat, S., & Kockarts, G. (2002). Response of the mesosphere to human-induced perturbations and solar variability calculated by a 2-D model. *Journal of Geophysical Research*, *107*(D18), 4358. https://doi.org/10.1029/2001JD001235

Kolstad, E. W., Wulff, C. O., Domeisen, D., & Woolings, T. (2020). Tracing North Atlantic Oscillation forecast errors to stratospheric origins. *Journal of Climate*, *33*(21), 9145–9157. https://doi.org/10.1175/JCLI-D-20-0270.1

Labitzke, K. (1982). On the interannual variability of the middle stratosphere during the northern winters. *Journal of the Meteorological Society of Japan*, *60*(1), 124–139. https://doi.org/10.2151/jmsj1965.60.1_124

Laboratory for Atmospheric and Space Physics. (2005). LASP Interactive Solar Irradiance Datacenter [Dataset]. *Laboratory for Atmospheric and Space Physics*. https://doi.org/10.25980/L27Z-XD34

Laskar, F. I., Chau, J. L., Stober, G., Hoffmann, P., Hall, C. M., & Tsutsumi, M. (2016). Quasi-biennial oscillation modulation of the middle- and high-latitude mesospheric semidiurnal tides during August–September. *Journal of Geophysical Research: Space Physics*, *121*(5), 4869–4879. https://doi.org/10.1002/2015JA022065

Laskar, F. I., Pallamraju, D., & Veenadhari, B. (2014). Vertical coupling of atmospheres: Dependence on strength of sudden stratospheric warming and solar activity. *Earth Planets and Space*, *66*(1), 94. https://doi.org/10.1186/1880-5981-66-94

Laštovička, J. (2005). On the role of solar and geomagnetic activity in long-term trends in the atmosphere–ionosphere system. *Journal of Atmospheric and Solar-Terrestrial Physics*, *67*(1), 83–92. https://doi.org/10.1016/j.jastp.2004.07.019

Laštovička, J., Akmaev, R. A., Beig, G., Bremer, J., Emmert, J. T., Jacobi, C., et al. (2008). Emerging pattern of global change in the upper atmosphere and ionosphere. *Annales Geophysicae*, *26*(5), 1255–1268. https://doi.org/10.5194/angeo-26-1255-2008

Lieberman, R. S., Riggin, D. M., Ortland, D. A., Nesbitt, S. W., & Vincent, R. A. (2007). Variability of mesospheric diurnal tides and tropospheric diurnal heating during 1997–1998. *Journal of Geophysical Research*, *112*(D20), D20110. https://doi.org/10.1029/2007JD008578

Lieberman, R. S., Smith, A. K., Franke, S. J., Vincent, R. A., Isler, J. R., Manson, A. H., et al. (2000). Comparison of mesospheric and lower thermospheric residual wind with High Resolution Doppler Imager, medium frequency, and meteor radar winds. *Journal of Geophysical Research*, *105*(D22), 27023–27035. https://doi.org/10.1029/2000JD900363

Lindzen, R., & Chapman, S. (1969). Atmospheric tides. *Space Science Reviews*, *10*(1), 3–188. https://doi.org/10.1007/bf00171584

Lindzen, R. S. (1978). Effect of daily variations of cumulonimbus activity on the atmospheric semidiurnal tide. *Monthly Weather Review*, *106*(4), 526–533. https://doi.org/10.1175/1520-0493(1978)106<0526:EODVOC>2.0.CO;2

Liu, H., Sun, Y.-Y., Miyoshi, Y., & Jin, H. (2017). ENSO effects on MLT diurnal tides: A 21 year reanalysis data-driven GAIA model simulation. *Journal of Geophysical Research: Space Physics*, *122*(5), 5539–5549. https://doi.org/10.1002/2017JA024011

Liu, H., Tao, C., Jin, H., & Nakamoto, Y. (2020). Circulation and tides in a cooler upper atmosphere: Dynamical effects of CO_2 doubling. *Geophysical Research Letters*, *47*(10), e2020GL087413. https://doi.org/10.1029/2020GL087413

Liu, H.-L., Wang, W., Richmond, A. D., & Roble, R. G. (2010). Ionospheric variability due to planetary waves and tides for solar minimum conditions. *Journal of Geophysical Research*, *115*(A6), A00G01. https://doi.org/10.1029/2009JA015188

López-González, M. J., Rodríguez, E., García-Comas, M., López-Puertas, M., Olivares, I., Shepherd, M. G., et al. (2017). Semidiurnal tidal activity of the middle atmosphere at mid-latitudes derived from O_2 atmospheric and OH(6–2) airglow SATI observations. *Journal of Atmospheric and Solar-Terrestrial Physics*, *164*, 116–126. https://doi.org/10.1016/j.jastp.2017.08.014

Lu, H., Pancheva, D., Mukhtarov, P., & Cnossen, I. (2012). QBO modulation of traveling planetary waves during northern winter. *Journal of Geophysical Research*, *117*(D9), D09104. https://doi.org/10.1029/2011JD016901

Manson, A. H., Luo, Y., & Meek, C. (2002). Global distributions of diurnal and semi-diurnal tides: Observations from HRDI-UARS of the MLT region. *Annales Geophysicae*, *20*(11), 1877–1890. https://doi.org/10.5194/angeo-20-1877-2002

Manson, A. H., Meek, C., Hagan, M. E., Zhang, X., & Luo, Y. (2004). Global distributions of diurnal and semidiurnal tides: Observations from HRDI-UARS of the MLT region and comparisons with GSWM-02 (migrating, nonmigrating components). *Annales Geophysicae*, *22*(5), 1529–1548. https://doi.org/10.5194/angeo-22-1529-2004

Marsh, D., & Russell, J. M. (2000). A tidal explanation for the sunrise/sunset anomaly in HALOE low-latitude nitric oxide observations. *Geophysical Research Letters*, *27*(19), 3197–3200. https://doi.org/10.1029/2000GL000070

Matsuno, T. (1971). A dynamical model of the stratospheric sudden warming. *Journal of the Atmospheric Sciences*, *28*(8), 1479–1494. https://doi.org/10.1175/1520-0469(1971)028<1479:ADMOTS>2.0.CO;2

McIntyre, M. E. (1982). How well do we understand the dynamics of stratospheric warming? *Journal of the Meteorological Society of Japan*, *60*(1), 37–65. https://doi.org/10.2151/jmsj1965.60.1_37

McLandress, C. (2002). Interannual variations of the diurnal tide in the mesosphere induced by a zonal-mean wind oscillation in the tropics. *Geophysical Research Letters*, *29*(9). https://doi.org/10.1029/2001GL014551

Merzlyakov, E. G., Portnyagin, Y. I., Jacobi, C., Mitchell, N. J., Muller, H. G., Manson, A. H., et al. (2001). On the longitudinal structure of the transient day-to-day variation of the semidiurnal tide in the mid-latitude lower thermosphere—I. Winter season. *Annales Geophysicae*, *19*(5), 545–562. https://doi.org/10.5194/angeo-19-545-2001

Mitchell, N. J. (2019). University of Bath: Esrange Skiymet meteor radar data—Catalogue.ceda.ac.UK [Dataset]. *CEDA*. Retrieved from https://catalogue.ceda.ac.uk/uuid/ba34cd217a8c49548f6fe62254b79fac/

Mitchell, N. J., Pancheva, D., Middleton, H. R., & Hagan, M. (2002). Mean winds and tides in the Arctic mesosphere and lower thermosphere. *Journal of Geophysical Research*, *107*(A1), 1004. https://doi.org/10.1029/2001JA900127

Miyahara, S., Miyoshi, Y., & Yamashita, K. (1999). Variations of migrating and nonmigrating tides simulated by the middle atmosphere circulation model at Kyushu University. *Advances in Space Research*, *24*(11), 1549–1558. https://doi.org/10.1016/s0273-1177(99)00879-0

National Oceanic and Atmospheric Administration. (2023a). NOAA Climate Prediction Center [Dataset]. *National Oceanic and Atmospheric Administration*. Retrieved from https://www.cpc.ncep.noaa.gov/products/precip/CWlink/pna/norm.nao.monthly.b5001.current.ascii.table

National Oceanic and Atmospheric Administration. (2023b). NOAA Global Monitoring Laboratory [Dataset]. *National Oceanic and Atmospheric Administration*. Retrieved from https://gml.noaa.gov/webdata/ccgg/trends/co2/co2_mm_gl.txt

National Oceanic and Atmospheric Administration. (2023c). NOAA Physical Sciences Laboratory [Dataset]. *National Oceanic and Atmospheric Administration*. Retrieved from https://psl.noaa.gov/data/timeseries/month/data/nino34.long.data

Oberheide, J., Forbes, J. M., Zhang, X., & Bruinsma, S. L. (2011). Climatology of upward propagating diurnal and semidiurnal tides in the thermosphere. *Journal of Geophysical Research*, *116*(A11), A11306. https://doi.org/10.1029/2011JA016784

Oberheide, J., Hagan, M. E., Roble, R. G., & Offermann, D. (2002). Sources of nonmigrating tides in the tropical middle atmosphere. *Journal of Geophysical Research*, *107*(D21), 4567. https://doi.org/10.1029/2002JD002220

Pancheva, D., Mitchell, N., Middleton, H., & Muller, H. (2003). Variability of the semidiurnal tide due to fluctuations in solar activity and total ozone. *Journal of Atmospheric and Solar-Terrestrial Physics*, *65*(1), 1–19. https://doi.org/10.1016/s1364-6826(02)00084-6

Pancheva, D., Mitchell, N. J., Hagan, M. E., Manson, A. H., Meek, C. E., Luo, Yi., et al. (2002). Global-scale tidal structure in the mesosphere and lower thermosphere during the PSMOS campaign of June–August 1999 and comparisons with the global scale wave model. *Journal of Atmospheric and Solar-Terrestrial Physics*, *64*, 1011–1035. https://doi.org/10.1016/S1364-6826(02)00054-8

Pancheva, D., & Mukhtarov, P. (2011). Atmospheric tides and planetary waves: Recent progress based on SABER/TIMED temperature measurements (2002–2007). In M. Abdu & D. Pancheva (Eds.), *Aeronomy of the Earth's atmosphere and ionosphere, IAGA Special Sopron Book Series (2)*. Springer.

Pancheva, D., Mukhtarov, P., & Andonov, B. (2009). Global structure, seasonal and interannual variability of the migrating semidiurnal tide seen in the SABER/TIMED temperatures (2002–2007). *Annales Geophysicae*, *27*(2), 687–703. https://doi.org/10.5194/angeo-27-687-2009

Pancheva, D., Mukhtarov, P., & Smith, A. K. (2013). Climatology of the migrating terdiurnal tide (TW3) in SABER/TIMED temperatures. *Journal of Geophysical Research: Space Physics*, *118*(4), 1755–1767. https://doi.org/10.1002/jgra.50207

Pancheva, D. V., & Mitchell, N. J. (2004). Planetary waves and variability of the semidiurnal tide in the mesosphere and lower thermosphere over Esrange (68°N, 21°E) during winter. *Journal of Geophysical Research*, *109*(A8), A08307. https://doi.org/10.1029/2004JA010433

Pedatella, N. M., & Forbes, J. M. (2010). Evidence for stratosphere sudden warming-ionosphere coupling due to vertically propagating tides. *Geophysical Research Letters*, *37*(11), L11104. https://doi.org/10.1029/2010GL043560

Pedatella, N. M., Fuller-Rowell, T., Wang, H., Jin, H., Miyoshi, Y., Fujiwara, H., et al. (2014). The neutral dynamics during the 2009 sudden stratosphere warming simulated by different whole atmosphere models. *Journal of Geophysical Research: Space Physics*, *119*(2), 1306–1324. https://doi.org/10.1002/2013JA019421

Pedatella, N. M., & Liu, H.-L. (2012). Tidal variability in the mesosphere and lower thermosphere due to the El Niño–Southern Oscillation. *Geophysical Research Letters*, *39*(19), L19802. https://doi.org/10.1029/2012GL053383

Pedatella, N. M., Liu, H.-L., Conte, J. F., Chau, J. L., Hall, C., Jacobi, C., et al. (2021). Migrating semidiurnal tide during the September equinox transition in the Northern Hemisphere. *Journal of Geophysical Research: Atmospheres*, *126*(3), e2020JD033822. https://doi.org/10.1029/2020JD033822

Pedatella, N. M., Liu, H.-L., Richmond, A. D., Maute, A., & Fang, T.-W. (2012). Simulations of solar and lunar tidal variability in the mesosphere and lower thermosphere during sudden stratosphere warmings and their influence on the low-latitude ionosphere. *Journal of Geophysical Research*, *117*(A8), A08326. https://doi.org/10.1029/2012JA017858

Ramesh, K., Mitchell, N. J., Hindley, N. P., & Moffat-Griffin, T. (2024). Long-term variability and tendencies in mesosphere and lower thermosphere winds from meteor radar observations over Esrange (67.9°N, 21.1°E). *Journal of Geophysical Research: Atmospheres*, *129*(7), e2023JD040404. https://doi.org/10.1029/2023JD040404

Ramesh, K., & Smith, A. K. (2021). Long-term variability and tendencies in non-migrating diurnal tide from WACCM6 simulations during 1850–2014. *Journal of Geophysical Research: Space Physics*, *126*(3), e2020JA028904. https://doi.org/10.1029/2020JA028904

Ramesh, K., Smith, A. K., Garcia, R. R., Marsh, D. R., Sridharan, S., & Kishore Kumar, K. (2020). Long-term variability and tendencies in migrating diurnal tide from WACCM6 simulations during 1850–2014. *Journal of Geophysical Research: Atmospheres*, *125*(23), e2020JD033644. https://doi.org/10.1029/2020JD033644

Riggin, D. M., Meyer, C. K., Fritts, D. C., Jarvis, M. J., Murayama, Y., Singer, W., et al. (2003). MF radar observations of seasonal variability of semidiurnal motions in the mesosphere at high northern and southern latitudes. *Journal of Atmospheric and Solar-Terrestrial Physics*, *65*(4), 483–493. https://doi.org/10.1016/S1364-6826(02)00340-1

Salminen, A., Asikainen, T., Maliniemi, V., & Mursula, K. (2020). Dependence of sudden stratospheric warmings on internal and external drivers. *Geophysical Research Letters*, *47*(5), e2019GL086444. https://doi.org/10.1029/2019GL086444

Sassi, F., Kinnison, D., Boville, B. A., Garcia, R. R., & Roble, R. (2004). Effect of El Niño–Southern Oscillation on the dynamical, thermal, and chemical structure of the middle atmosphere. *Journal of Geophysical Research*, *109*(D17), D17108. https://doi.org/10.1029/2003JD004434

Schimanke, S., Spangehl, T., Huebener, H., & Cubasch, U. (2013). Variability and trends of major stratospheric warmings in simulations under constant and increasing GHG concentrations. *Climate Dynamics*, *40*(7–8), 1733–1747. https://doi.org/10.1007/s00382-012-1530-x

Schmidt, H., Brasseur, G. P., Charron, M., Manzini, E., Giorgetta, M. A., Diehl, T., et al. (2006). The HAMMONIA chemistry climate model: Sensitivity of the mesopause region to the 11-year solar cycle and CO_2 doubling. *Journal of Climate*, *19*(16), 3903–3931. https://doi.org/10.1175/jcli3829.1

Shepherd, G., Roble, R. G., Zhang, S.-P., McLandress, C., & Wiens, R. H. (1998). Tidal influence on midlatitude airglow: Comparison of satellite and ground-based observations with time-GCM predictions. *Journal of Geophysical Research*, *103*(A7), 14741–14751. https://doi.org/10.1029/98JA00884

Siddiqui, T. A., Maute, A., & Pedatella, N. M. (2019). On the importance of interactive ozone chemistry in Earth-System models for studying mesophere-lower thermosphere tidal changes during sudden stratospheric warmings. *Journal of Geophysical Research: Space Physics*, *124*(12), 10690–10707. https://doi.org/10.1029/2019JA027193

Smith, A. K. (2000). Structure of the terdiurnal tide at 95 km. *Geophysical Research Letters*, *27*(2), 177–180. https://doi.org/10.1029/1999GL010843

Smith, A. K. (2012). Global dynamics of the MLT. *Surveys in Geophysics*, *33*(6), 1177–1230. https://doi.org/10.1007/s10712-012-9196-9

Smith, A. K., Marsh, D. R., & Szymczak, A. C. (2003). Interaction of chemical heating and the diurnal tide in the mesosphere. *Journal of Geophysical Research*, *108*(D5), 4164. https://doi.org/10.1029/2002JD002664

Smith, A. K., Pancheva, D. V., Mitchell, N. J., Marsh, D. R., Russell, J. M., III., & Mlynczak, M. G. (2007). A link between variability of the semidiurnal tide and planetary waves in the opposite hemisphere. *Geophysical Research Letters*, *34*(7), L07809. https://doi.org/10.1029/2006GL028929

Sofieva, V. F., Kalakoski, N., Verronen, P. T., Päivärinta, S.-M., Kyrölä, E., Backman, L., & Tamminen, J. (2012). Polar-night O_3, NO_2 and NO_3 distributions during sudden stratospheric warmings in 2003–2008 as seen by GOMOS/Envisat. *Atmospheric Chemistry and Physics*, *12*(2), 1051–1066. https://doi.org/10.5194/acp-12-1051-2012

Sprenger, K., & Schminder, R. (1969). Solar cycle dependence of winds in the lower ionosphere. *Journal of Atmospheric and Terrestrial Physics*, *31*(1), 217–221. https://doi.org/10.1016/0021-9169(69)90100-7

Sridharan, S., Sathishkumar, S., & Gurubaran, S. (2012). Variabilities of mesospheric tides during sudden stratospheric warming events of 2006 and 2009 and their relationship with ozone and water vapour. *Journal of Atmospheric and Solar-Terrestrial Physics*, *78*(79), 108–115. ISSN 1364–6826. https://doi.org/10.1016/j.jastp.2011.03.013

Sun, R., Gu, S., Dou, X., & Li, N. (2022). Tidal structures in the mesosphere and lower thermosphere and their solar cycle variations. *Atmosphere*, *13*(12), 2036. https://doi.org/10.3390/atmos13122036

Sundararajan, S. (2020). Equatorial upper mesospheric mean winds and tidal response to strong El Niño and La Niña. *Journal of Atmospheric and Solar-Terrestrial Physics*, *202*, 105270. https://doi.org/10.1016/j.jastp.2020.105270

Trenberth, K. E., Caron, J. M., Stepaniak, D. P., & Worley, S. (2002). Evolution of El Niño–Southern Oscillation and global atmospheric surface temperatures. *Journal of Geophysical Research*, *107*(D8). https://doi.org/10.1029/2000JD000298

Vadas, S. L., Liu, H.-L., & Lieberman, R. S. (2014). Numerical modeling of the global changes to the thermosphere and ionosphere from the dissipation of gravity waves from deep convection. *Journal of Geophysical Research: Space Physics*, *119*(9), 7762–7793. https://doi.org/10.1002/2014JA020280

van Caspel, W. E., Espy, P. J., Ortland, D. A., & Hibbins, R. E. (2022). The mid- to high-latitude migrating semidiurnal tide: Results from a mechanistic tide model and SuperDARN observations. *Journal of Geophysical Research: Atmospheres*, *127*(1), e2021JD036007. https://doi.org/10.1029/2021JD036007

Ward, W. E. (1999). A simple model of diurnal variations in the mesospheric oxygen nightglow. *Geophysical Research Letters*, *26*(23), 3565–3568. https://doi.org/10.1029/1999GL003661

Ward, W. E., Fomichev, V. I., & Beagley, S. (2005). Nonmigrating tides in equinox temperature fields from the Extended Canadian Middle Atmosphere Model (CMAM). *Geophysical Research Letters*, *32*(3), L03803. https://doi.org/10.1029/2004GL021466

Warner, K., & Oberheide, J. (2014). Nonmigrating tidal heating and MLT tidal wind variability due to the El Niño–Southern Oscillation. *Journal of Geophysical Research: Atmospheres*, *119*(3), 1249–1265. https://doi.org/10.1002/2013JD020407

Wilks, D. S. (2006). *Statistical methods in the atmospheric sciences* (2nd ed.). Academic Press.

Wu, Q., Ortland, D. A., Killeen, T. L., Roble, R. G., Hagan, M. E., Liu, H., et al. (2008). Global distribution and interannual variations of mesospheric and lower thermospheric neutral wind diurnal tide: 1. Migrating tide. *Journal of Geophysical Research*, *113*(A5), A05308. https://doi.org/10.1029/2007JA012542

Wu, Q., Ortland, D. A., Solomon, S. C., Skinner, W. R., & Niciejewski, R. J. (2011). Global distribution, seasonal, and inter-annual variations of mesospheric semidiurnal tide observed by TIMED TIDI. *Journal of Atmospheric and Solar-Terrestrial Physics*, *73*(17–18), 2482–2502. https://doi.org/10.1016/j.jastp.2011.08.007

Yiğit, E., Medvedev, A. S., & Ern, M. (2021). Effects of latitude-dependent gravity wave source variations on the middle and upper atmosphere. *Frontiers in Astronomy and Space Sciences*, *7*, 614018. https://doi.org/10.3389/fspas.2020.614018

Yue, J., Xu, J., Chang, L. C., Wu, Q., Liu, H.-L. L., Lu, X., & Russell, J. (2013). Global structure and seasonal variability of the migrating terdiurnal tide in the mesosphere and lower thermosphere. *Journal of Atmospheric and Solar-Terrestrial Physics*, *105–106*, 191–198. https://doi.org/10.1016/j.jastp.2013.10.010

Zhang, L., & Chen, Q. (2019). Analysis of the variations in the strength and position of stratospheric sudden warming in the past three decades. *Atmospheric and Oceanic Science Letters*, *12*(3), 147–154. https://doi.org/10.1080/16742834.2019.1586267

Zhang, S. P. P., Roble, R. G., & Shepherd, G. G. (2001). Tidal influence on the oxygen and hydroxyl nightglows: Wind Imaging Interferometer observations and thermosphere-ionosphere-mesosphere electrodynamics general circulation model. *Journal of Geophysical Research*, *106*(A10), 21381–21393. https://doi.org/10.1029/2000ja000363

Zhao, X. R., Sheng, Z., Shi, H. Q., Weng, L. B., & Liao, Q. X. (2020). Long-term trends and solar responses of the mesopause temperatures observed by SABER during the 2002–2019 period. *Journal of Geophysical Research: Atmospheres*, *125*(11), e2020JD032418. https://doi.org/10.1029/2020JD032418